Quantitative Analysis of Synaptic Vesicle Membrane Trafficking

Dissertation

for the award of the degree

"Doctor rerum naturalium"

of the Georg-August-Universität Göttingen

within the doctoral program Molecular Biology

of the Georg-August University School of Science (GAUSS)

submitted by

Katharina Seitz

born in Munich

Göttingen, 2017

Examination Board

Thesis Committee

Prof. Dr. Silvio Rizzoli (Referee)

Institute for Neuro- and Sensory Physiology

University of Göttingen Medical Centre, Göttingen, Germany

PD Dr. Halyna Shcherbata (2nd Referee)

Research Group Gene Expression and Signaling

Max Planck Institute for Biophysical Chemistry, Göttingen, Germany

Prof. Dr. Michael Thumm

Institute for Cellular Biochemistry

University of Göttingen Medical Centre, Göttingen, Germany

Extended Examination Board

Dr. Camin Dean

Group of Trans-synaptic Signalling

European Neuroscience Institute, Göttingen, Germany

Prof. Dr. Peter Rehling

Department of Cellular Biochemistry

University of Göttingen Medical Centre, Göttingen, Germany

Prof. Dr. Blanche Schwappach

Department of Molecular Biology

University of Göttingen Medical Centre, Göttingen, Germany

Affidavit

I hereby declare that I prepared this dissertation independently, and with no other sources and aids than quoted.

Katharina Seitz

“The problem with pounding a square peg into a round hole is not that the hammering is hard work. It's that you're destroying the peg.”

- Paul Collins

Dedicated to my grandparents

and everyone who wouldn’t even dream of looking for a hammer.

Table of Contents

Acknowledgements

I would like to thank Professor Rizzoli for his guidance and supervision. Thanks also go to my thesis committee members, Professors Shcherbata and Thumm, for their help and fruitful discussions.

I'm grateful to all lab members, both current and former, for creating a pleasant work environment. Some of you have become so much more than colleagues, and although human interactions are not always without complications, I wouldn't trade any of them for the world. Thank you.

Most importantly, thank you, Sven, for being with me there and back again. I see you.

SUMMARY

The fate of synaptic vesicles upon fusion to the plasma membrane is unclear. Two models have been proposed: vesicle proteins either stay clustered in patches, thus retaining the molecular identity of individual vesicles, or they disintegrate and intersperse with other surface-resident proteins. Although this problem has been investigated in numerous studies, no consensus has been reached as to which of the models is true.

I developed a new method using single-domain antibodies and STED microscopy to selectively visualize newly exocytosed vesicle proteins, and determine changes in the sizes of vesicle protein clusters in the time of recovery after exocytosis. I applied the method to different proteins of interest in hippocampal neuronal cultures and *Drosophila melanogaster* neuromuscular junctions.

Using this single-domain antibody-based vesicle tracking assay, I could show that synaptophysin-pHluorin and synaptobrevin-pHluorin remain clustered on the plasma membrane of synaptic boutons for at least the first minute after exocytosis. Patches of synaptobrevin-pHluorin that diffuse into axonal plasma membrane segments, however, disintegrate during the same time frame. This indicates that in addition to already proposed mechanisms for maintenance of vesicle integrity, there may exist an additional mechanism that is inherent to the environment of synaptic boutons, as opposed to the vesicles themselves. A supporting endocytic scaffold might aid in clustering synaptic vesicle proteins.

1. INTRODUCTION

1.1 Synaptic vesicles and vesicle recycling

Synapses relay electrical signals (action potentials) from one neuron to the next via exocytosis of neurotransmitters. These are stored in so-called synaptic vesicles. Synaptic vesicles are well-described spherical organelles with a diameter of 40 to 60 nm. They are delimited by a cholesterol-rich lipid bilayer containing a multitude of proteins that are involved in vesicle exocytosis and recycling, and that have been extensively characterized and quantified (Takamori et al., 2006; Wilhelm et al., 2014). The most abundant of these synaptic vesicle proteins are the SNARE protein synaptobrevin (VAMP2), which is present in 70 copies per vesicle, and synaptophysin (31 copies per vesicle, Takamori et al., 2006).

Calcium influx triggered by membrane depolarization through an action potential leads to exocytosis of synaptic vesicles. The neurotransmitters they contain are released into the synaptic cleft, leaving them to modulate the postsynaptic membrane potential via ionotropic receptors. After exocytosis, synaptic vesicles remain on the plasma membrane for a certain amount of time (as the so-called surface pool of vesicles) before being retrieved and re-filled with neurotransmitters (reviewed by Rizzoli 2014).

1.2 Vesicle Integrity

There is no consensus on what happens to synaptic vesicles during the time they spend on the plasma membrane. Two models are conceivable. First, the dispersal model: synaptic vesicle proteins of newly exocytosed vesicles intermix with components of other surface pool vesicles, meaning that vesicles retrieved from the plasma membrane will have a different protein composition and thereby molecular identity than the originally exocytosed vesicles. Second, the cohesion model: vesicles stay organised in clusters on the plasma membrane, resulting in retrieval of the same vesicles that were exocytosed, meaning that vesicles retain their identity throughout their life cycle (Figure 1.1, reviewed by Opazo & Rizzoli, 2010). The question of which of these models applies has been addressed in multiple studies, and evidence for both models has been found.

Most of the evidence for the dispersal model stems from observations carried out with live epifluorescence microscopy experiments utilizing fluorescent fusion proteins.

Fernández-Alfonso et al. 2006 addressed the integrity problem using synaptobrevin-pHluorin (spH)-expressing neuronal cultures. The pHluorin moiety of the fusion construct is a pH sensitive variant of GFP that is fluorescent in neutral pH but becomes quenched in acidic environments such as the lumen of synaptic vesicles (Miesenböck, De Angelis, and Rothman 1998). Fernández-Alfonso and colleagues bleached surface-resident pHluorin molecules before stimulating exocytosis electrically. Due to new spH molecules being exocytosed, they

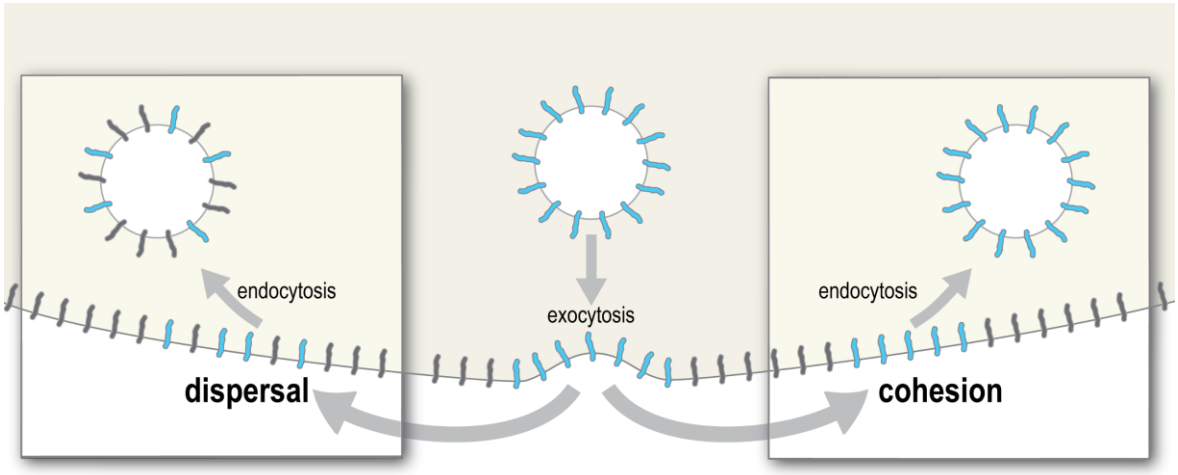

Figure 1.1. Models of vesicle integrity. After exocytosis, vesicle proteins either stay organized in clusters and are recycled maintaining their molecular identity (cohesion model), or diffuse apart and intermix with other surface-resident vesicle proteins, resulting in endocytosis of vesicles with different molecular identities from those that were exocytosed (dispersal model).

observed an increase in fluorescence upon stimulation. In the minutes after stimulation, fluorescence decreased again due to endocytosis of vesicles and subsequent quenching of the associated pHluorins. However, the fluorescence intensity did not return to the same values as after bleaching, but remained higher (Figure 1.2). The study concludes that this indicates intermixing of the components of newly exocytosed un-bleached and surface-resident bleached vesicles, and thereby endocytosis of vesicles with mixed compositions of bleached and un-bleached pHluorins. However, the assumption of intermixing is not necessary to explain their observations. It is equally possible that the incomplete return to baseline fluorescence stems from simultaneous uptake of vesicles consisting entirely of bleached and non-bleached pHluorins each.

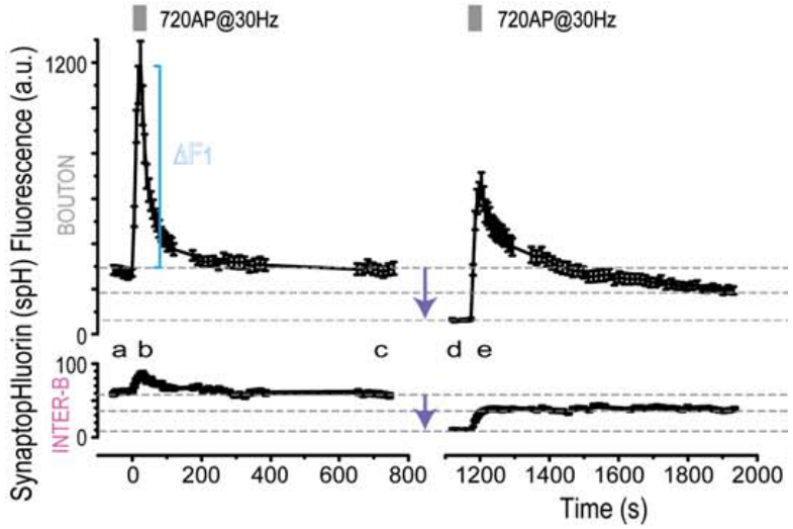

Figure 1.2. synaptopHluorin-based investigation of vesicle integrity. Synaptobrevin-pHluorin (spH)-expressing neurons were stimulated 2 times with 720 action potentials at 30 Hz (b and e). Between stimulations, surface-resident pHluorin molecules were bleached (violet arrows). Fluorescence after recovery from the second stimulation (t = 2000 s) does not return to baseline values (c). Adapted from Fernández-Alfonso et al. 2006

Another line of evidence that this study, and others, e.g. Granseth et al. 2006, and Sankaranarayanan and Ryan 2000 suggest as

indicative for the dispersion model of vesicle integrity stems from the observation that after stimulation of pHluorin expressing neurons, the fluorescence intensity in the axonal segments between synaptic boutons increases rapidly. The authors conclude this is due to rapid disintegration of vesicles and diffusion of vesicle components into the axons. However, the observation could be equally well explained by patches of vesicles diffusing into the axonal segments.

Wienisch and Klingauf performed very similar experiments to those of Fernández-Alfonso in 2006. Instead of eliminating fluorescence of surface pHluorin molecules by bleaching, they engineered a TEV protease cleavage site between the synaptobrevin and pHluorin moieties of the fusion construct, and removed surface-resident pHluorin by enzymatic cleavage. Their observations and conclusions agree with those of Fernández-Alfonso et al.: fluorescence intensities increase after stimulation and don't return to baseline during recovery, which to them indicates intermixing of vesicle components. However, as has been delineated above, the observations can equally well be explained by the cohesion model.

Super-resolution investigations of the synaptic vesicle integrity problem have mainly found evidence for the cohesion model.

In 2006, Willig et al. used antibodies to fluorescently label surface-resident synaptotagmin I proteins, and upon investigation with STED microscopy found that synaptotagmin was arranged in clusters on the plasma membrane that were of a size coinciding with that expected for synaptic vesicles, independent of preceding stimulation (Figure 1.3). Opazo et al. 2010 expanded on these findings by blocking surface-resident epitopes of synaptotagmin with a non-fluorescent antibody, and visualizing newly exocytosed vesicle populations with antibodies carrying different fluorescent labels, finding no evidence for intermixing of the vesicle populations. Finally, Hoopmann et al. 2010 analysed the degrees of correlation of newly exocytosed synaptotagmin molecules with all surface-resident synaptophysin

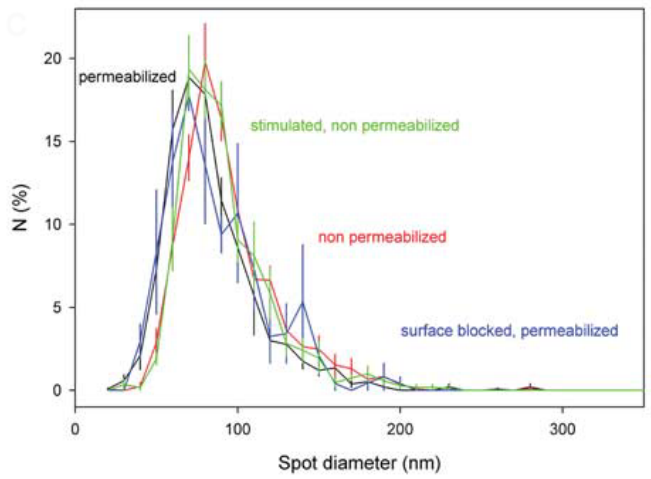

Figure 1.3 Investigation of vesicle size using STED microscopy. Neuronal cultures were stained with an antibody against the synaptic vesicle protein synaptotagmin I and visualized with STED micsocopy. There is no difference in apparent vesicle size between the complete vesicle complement of the synapse (permeabilized), the internal pool (surface blocked, permeabilized), the surface pool (non-permeabilized) and the surface pool after stimulation (stimulated, non-permeabilized), suggesting that synaptotagmin I stays clustered after exocytosis. Adapted from Willig et al. 2006

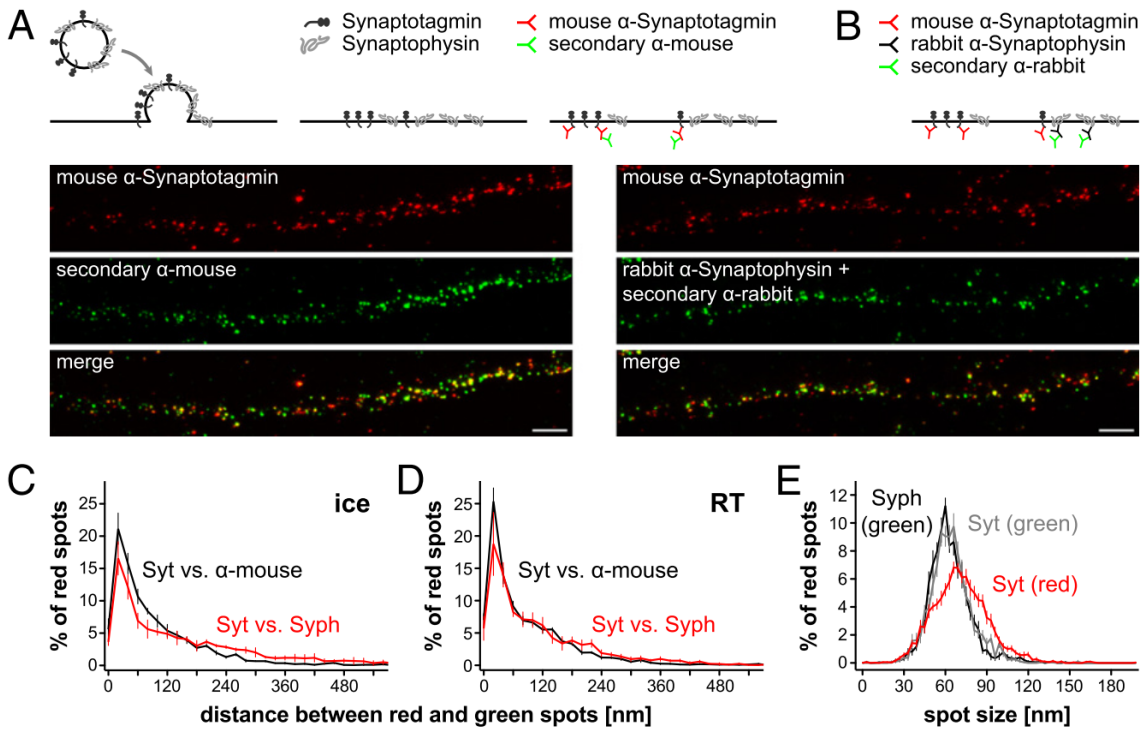

Figure 1.4 Investigation of vesicle protein colocalization with STED microscopy. Newly exocytosed synaptotagmin proteins were labelled by blocking surface epitopes with a non-fluorescent antibody and subsequently stimulating exocytosis in presence of a fluorescently labelled synaptoptagmin antibody. **A)** As a positive control for colocalization, the mouse anti-synaptotagmin antibody (red) was labelled with a secondary anti-mouse antibody (green). **B)** In addition to the newly exocytosed synaptotagmin proteins, surface-resident synaptophysin was labelled with a synaptophysin antibody from rabbit, and a corresponding secondary antibody (green). **C-D)** The colocalization between synaptotagmin and synaptophysin is not significantly different compared to the positive control, both on ice and at room temperature**. E)** Sizes of fluorescent spots produced by synaptotagmin and synaptophysin labelling do not differ significantly. Adapted from Hoopmann et al. 2010.

molecules, finding that almost no synaptotagmin molecules had escaped synaptic vesicle patches, and concluding that newly exocytosed synaptotagmin and synaptophysin remain clustered upon exocyctosis (Figure 1.4).

All of these studies used IgG antibodies for labelling the vesicle proteins of interest, which leaves them open to criticism regarding the potential for artificially induced clustering of epitopes due to the multivalency of antibodies (Fornasiero and Opazo 2015). Additionally, they only represent single moments in time, whereas observation of the behavior of synaptic vesicles on the plasma membrane over a certain defined time span after their exocytosis would present more stringent information about the fate of synaptic vesicles upon fusion.

1.3 A single-domain antibody-based method for investigating the integrity problem

The aim of my thesis was to use single-domain antibodies (sdAbs, also known as nanobodies®) to track newly exocytosed vesicles using super-resolution microscopy by improving on the approach of Hoopmann et al. in 2010: the blocking of surface epitopes with an unlabeled affinity probe, and using a fluorescently labelled version of the same probe to label un-blocked epitopes that become available after stimulation of exocytosis. Contrary to Hoopmann et al., my goal was not to measure the degree of association of synaptic vesicle proteins with recently exocytosed vesicles, but to investigate changes in size of the recently exocytosed vesicles in the time course of recovery after stimulation, which is the most immediate measure for judging vesicle integrity.

Disadvantages of antibody-based assays for the examination of vesicle integrity

In 2010, when Hoopmann et al. performed their experiments, antibodies were the only affinity probes of which species detecting the luminal domains of vesicle proteins were readily available. However, antibodies are a suboptimal choice for investigating the matter at hand: first, since antibodies are comparably expensive, it might not be possible to apply them in a high enough excess to ensure blocking of all surface epitopes. Second, the large size of antibodies (10 nm) introduces the problem of steric hindrance, further hampering the ability of the probes to reach all epitopes. Indeed, Hoopmann et al. only succeeded in reducing fluorescence intensity from an antibody staining of surface-blocked neurons to approximately 10% of that from an un-blocked sample (Figure 1.5). Therefore, it cannot be assumed that all vesicle proteins they observed stemmed from vesicles exocytosed during the controlled stimulation they applied. The large size of antibodies also leads to displacement of the fluorophore from its target, possibly leading to the apparent size of the structure observed being significantly larger than its actual size (reviewed by Maidorn, Rizzoli, & Opazo, 2016). Especially when investigating objects as small as plasma membrane resident synaptic vesicles

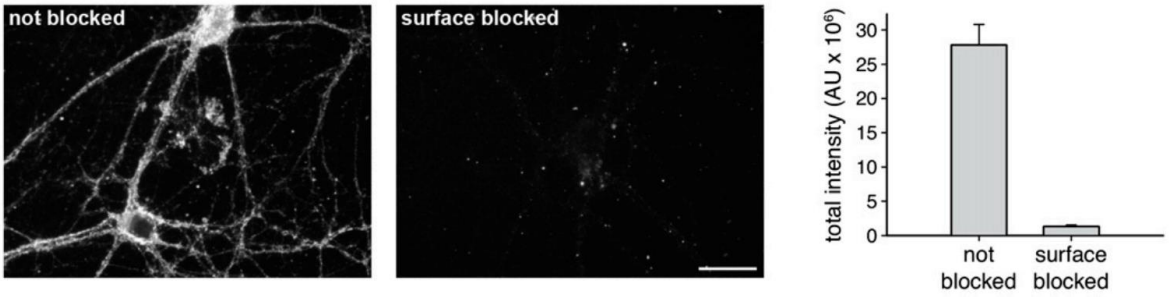

Figure 1.5. Blocking of surface epitopes by not fluorescently-conjugated antibodies. Hippocampal neuronal cultures were stained with an Atto647N-labelled anti-synaptotagmin antibody without ("not blocked") or with ("surface blocked") preceding application of an unlabeled antibody of the same species. Adapted from Hoopmann et al. 2010

(~90 nm when fully collapsed into the membrane) with the goal of making statements about changes in their size, this is a problem to be avoided at all cost.

Suitability of sdAbs for investigating synaptic vesicle integrity

The size of sdAbs (2 nm) is much smaller than that of antibodies. As has been demonstrated in multiple studies, the labelling density reached in immunostainings carried out with sdAbs is much higher than that of antibody stainings (reviewed by Maidorn et al., 2016). Blocking of surface-resident epitopes of synaptic vesicle proteins with sdAbs that are not fluorescently labelled, and labelling of newly exocytosed vesicles by their fluorescent counterparts, can therefore be assumed to be much more comprehensive compared to the use of antibodies as well.

The monovalence of sdAbs eliminates an additional possible source of bias specific to the vesicle integrity problem: contrarily to assays performed with probes that bind multiple epitopes at the same time (such as divalent IgG antibodies), when using sdAbs, potential artificial clustering of proteins by the probe, which could lead to evidence falsely supporting the cohesion model, can be excluded.

Additionally, sdAbs can be engineered in a way that renders it possible to fluorescently conjugate them to exactly one fluorophore per sdAb molecule. By contrast, antibodies are usually conjugated to fluorophores by N-hydroxysuccinimide ester coupling, which attaches fluorophores to all accessible amino groups of the antibody protein. The efficiency of this reaction is difficult to predict, which means that it cannot be determined how many fluorophores are coupled to a single antibody. When using sdAbs labelled with exactly one fluorophore to track newly exocytosed vesicles, the fluorescence intensity of the labelled vesicle patches can be semi-quantitatively used as a measure for the number of proteins in the patch, and therefore serves as an additional source of information for judging the integrity of synaptic vesicles.

Considerations for the use of an sdAb against GFP for visualizing newly exocytosed vesicles

Ideally, for labelling newly exocytosed vesicles, one would employ sdAbs targeting the luminal domains of synaptic vesicle proteins. However, no such sdAbs are available yet. An alternative is the use of proteins that are tagged with GFP at their luminal domains, which are readily available in the form of pHluorin-tagged proteins (reviewed e.g. by Dreosti & Lagnado, 2011), and perform the labelling with an sdAb against GFP ($sdAb_{GFP,}$ Rothbauer et al., 2006). This also provides several advantages: the assay is readily transferrable to any model system capable of expressing GFP-tagged proteins. Additionally, the use of the same probe for all proteins eliminates possible bias introduced by different affinities of the probes to their target proteins (as described by Ries et al. 2012).

Scope of this thesis

In this work, I present an assay using $sdAb_{GFP}$ to track newly exocytosed synaptic vesicles (Figure 1.6). Fluorescently unconjugated $sdAb_{GFP}$ is applied to a biological specimen expressing synaptophysin-pHluorin (sypHy, Granseth et al. 2006), or synaptobrevin-pHluorin (spH, Miesenböck et al. 1998, Sankaranarayanan & Ryan, 2001) to block all surface-resident epitopes. Subsequently, exocytosis of synaptic vesicles is evoked and the newly exocytosed vesicles are labelled by an $sdAb_{GFP}$ fluorescently conjugated to Atto647N ($sdAb_{GFP}$*), a dye suitable for STED microscopy.

I show that the method can be successfully used to observe newly exocytosed vesicles in hippocampal neuronal cultures expressing sypHy and spH, as well as preparations of *Drosophila melanogaster* larval neuromuscular junctions (dNMJ) expressing spH.

Additionally, I demonstrate that sypHy and spH protein clusters on the plasma membrane of synaptic boutons do not disintegrate during recovery after stimulation, but clusters of spH proteins that move to inter-bouton axonal segments do lose their integrity during the same time frame.

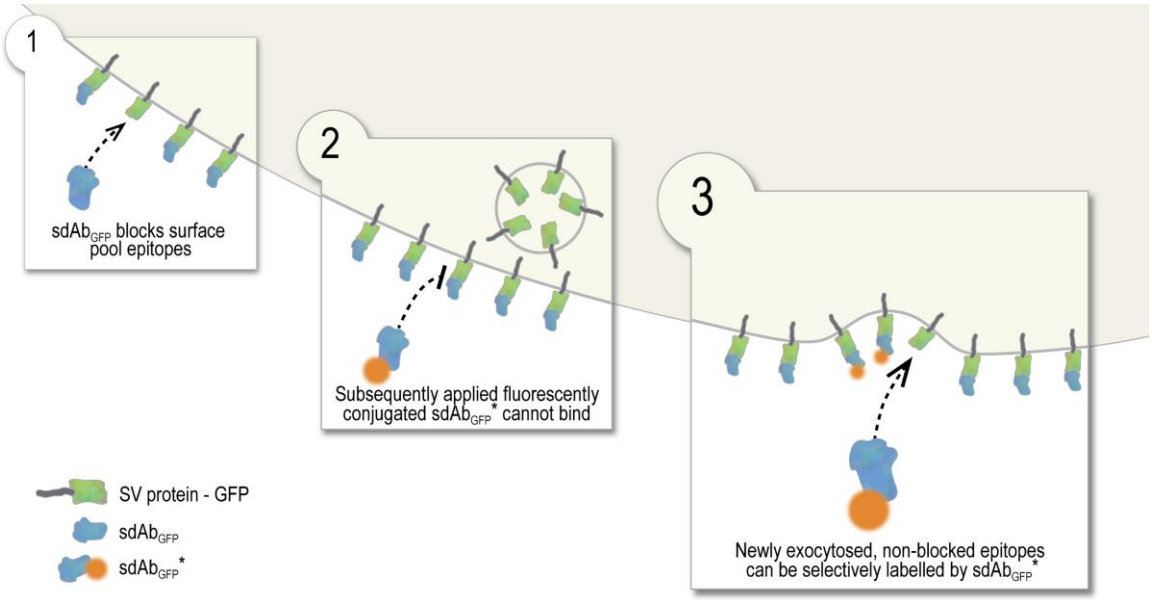

Figure 1.6. A nanobody-based assay to selectively observe newly exocytosed vesicles. Neurons expressing vesicle proteins fused to GFP at their luminal domain are exposed to not fluorescently conjugated $sdAb_{GFP}$ (1), resulting in surface epitopes of GFP being inaccessible to subsequently applied $sdAb_{GFP}$* (2). Upon stimulation of exocytosis, new epitopes become available that can be bound by $sdAb_{GFP}$*, thus allowing for the selective labelling of newly exocytosed vesicle proteins (3).

2. RESULTS

2.1 Optimization of tracking assay paramters

To implement the sdAb-based assay to track newly exocytosed synaptic vesicles, the following points needed to be established: the concentration of $sdAb_{GFP}$ applied for blocking all GFP epitopes on the cell surface; the application of $sdAb_{GFP}$* for fluorescently labelling the newly available epitopes after exocytosis; and the set of stimulation paradigms and time courses that will yield the most meaningful results.

Concentration of $sdAb_{GFP}$ applied for blocking surface epitopes

To make the observation of newly exocytosed vesicles with the described tracking assay possible, it is essential that all $sdAb_{GFP}$ epitopes of surface pool vesicles are occupied by $sdAb_{GFP}$. Only then can it be assumed that all vesicles that are visualized with $sdAb_{GFP}$* after a controlled stimulation train are vesicles that were exocytosed during that stimulation train.

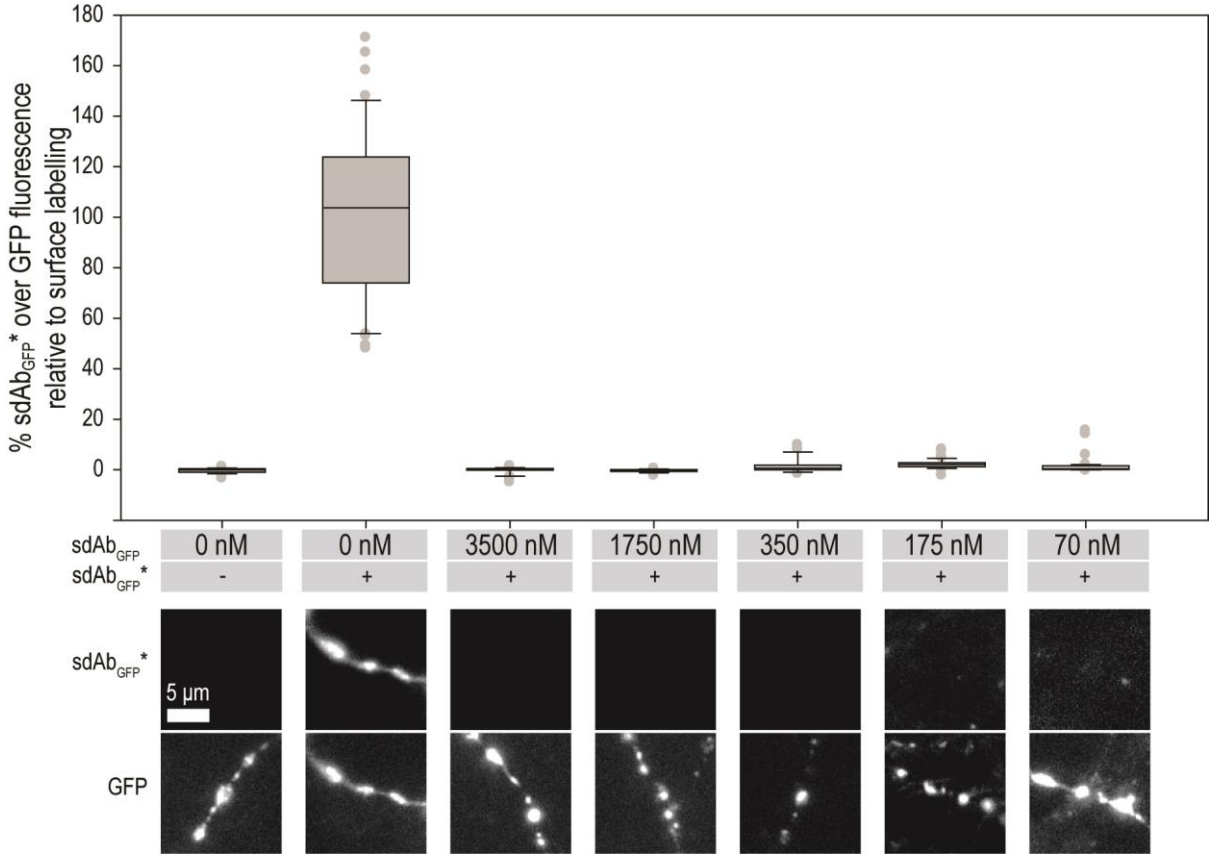

Figure 2.1 Blocking of surface-resident GFP epitopes of synapses in neuronal cultures expressing sypHy. Preparations were incubated with $sdAb_{GFP}$ for 5 min in the concentrations indicated, washed briefly, and stained with $sdAb_{GFP}$* for 2 minutes. Y-axes indicate the ratio of $sdAb_{GFP}$* fluorescence over GFP fluorescence in synaptic boutons, relative to complete surface labelling. N ≥ 22 synapses each. Epifluorescence images, scale bar 5 µm.

To ensure complete blocking of all surface epitopes, the concentration of $sdAb_{GFP}$ applied to the samples needs to be carefully chosen. Therefore, I incubated neuronal cultures expressing synaptophysin-pHluorin (sypHy) with $sdAb_{GFP}$ in several different concentrations, before washing and staining with $sdAb_{GFP}$* (Figure 2.1). As a negative control for blocking, I incubated with buffer instead of $sdAb_{GFP}$, which results in a complete surface labelling by $sdAb_{GFP}$*. As a positive control, I additionally did not apply $sdAb_{GFP}$*. A good measure for the effectiveness of blocking is the ratio of the fluorescence intensity of $sdAb_{GFP}$* to GFP compared to the controls. If the blocking of surface epitopes is successful, the $sdAb_{GFP}$*/GFP fluorescence ratio should approach that of the positive control. The more epitopes remain un-blocked, the more the ratio would approach that of the negative control/complete surface labelling.

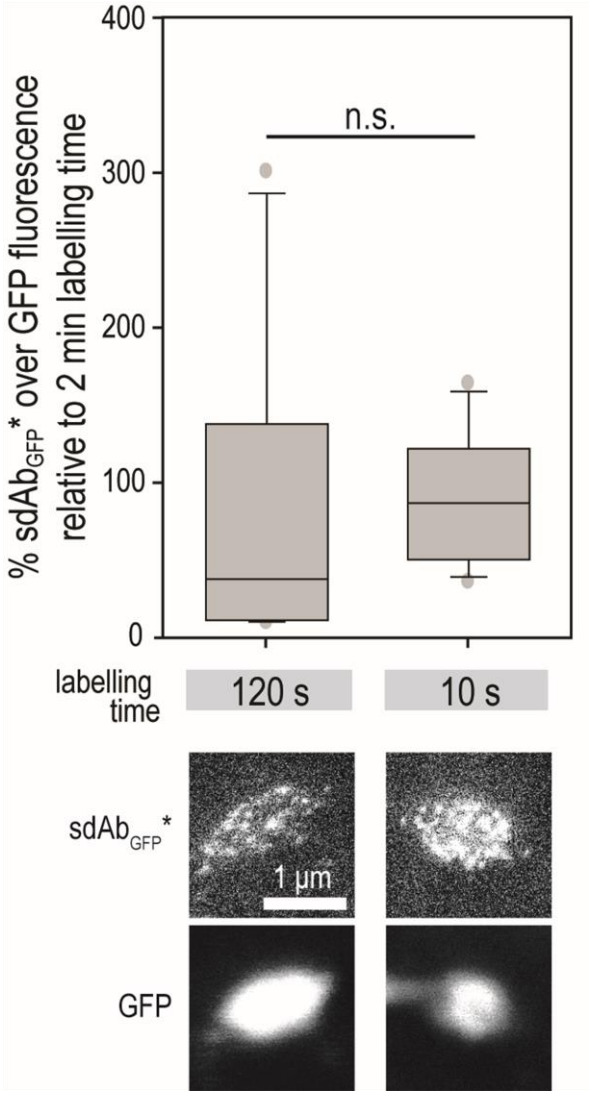

Figure 2.2 Live staining of surface-resident GFP molecules. Neuronal cultures were incubated with $sdAb_{GFP}$* for 120 s or 10 s, washed briefly and fixed. Y-axis indicates the ratio of $sdAb_{GFP}$* fluorescence over GFP fluorescence in synaptic boutons, relative to 120 s incubation time. N ≥ 17 synapses each. STED ($sdAb_{GFP}$*) and confocal (GFP) images, scale bar 1 µm.

As evident from Figure 2.1, complete blocking of surface epitopes is reached with $sdAb_{GFP}$ concentrations ranging from 3500 nM to 175 nM. In neurons treated with 70 nM $sdAb_{GFP}$, a small number of synapses appeared to have some unblocked epitopes. Therefore, I chose to use 175 nM $sdAb_{GFP}$ for future experiments.

Duration of $sdAb_{GFP}$ labelling*

In the experiments optimizing $sdAb_{GFP}$ blocking concentrations, labelling with $sdAb_{GFP}$* was carried out for two minutes. However, since the goal of this work was to observe vesicles at precise time points in the seconds to minute range after their exocytosis, and labelling times should be constant for all conditions, it is desirable to keep the labelling time as short as possible. Figure 2.2 shows the $sdAb_{GFP}$*/GFP fluorescence ratio in live surface stainings of neurons expressing sypHy, with labelling times of 120 s and 10 s. Since there is no significant

difference between the two conditions, I limited the incubation time with $sdAb_{GFP}$* to 10 s for future experiments.

Experimental conditions in neuronal cultures

For the choice of the stimulation paradigms applied and the exact time points of observation (i. e. washing and application of ice cold fixative to the sample) after stimulation, several factors need to be taken into account in order to ensure meaningful results.

First, the time spans of interest should be longer than the time required for labelling and transfer of the sample to the fixative (10 s plus approximately 5 s).

Second, the last time point of interest should not be so late that most of the recently exocytosed vesicles have already been endocytosed again. Inhibiting endocytosis for the entire recovery time to circumvent this problem (e.g. by incubating on ice or in absence of divalent ions) would be unfavourable, since it would also interfere with the behaviour of the vesicles - for example, reduced diffusion rates due to cold temperatures could lead to results falsely supporting the cohesion model. The process of clathrin-mediated endocytosis itself operates at a time constant of 20-30 s (Ryan et al. 1996, Rizzoli 2014) and appears to vary with the strength of the preceding stimulus (Wu and Betz 1996), while almost the entire surface pool of vesicles has been shown to be internalized within 5 minutes after a single labelling event (Westphal et al. 2008). There is also considerable evidence that vesicles that were already part of the surface pool at the time of a stimulation event are endocytosed preferentially over those exocytosed during that stimulation event (Wienisch and Klingauf 2006). Summarizing, it seems safe to assume that 60 s after a stimulation train, a considerable number of vesicles that were exocytosed during that train will still be present on the surface of the synapse.

Third, the electrical stimulation applied should be sufficiently great to release a noteworthy number of vesicles, while also not being so harsh as to release too many vesicles, in which case the chances of observing single vesicles instead of clusters would decline. Electrical stimulation of hippocampal cultures at a frequency of 20 Hz for 3 s (corresponding to 60 AP) releases vesicles of the readily releasable pool, while stimulation for 30 s at 20 Hz (600 AP) leads to the release of the entire recycling pool.

Considering these points, I chose to stimulate my cultures for 10 s at 20 Hz (~ 200 AP), and fluorescently label and fix them either directly after stimulation, or after a recovery time of 30 s and 60 s. Labelling with $sdAb_{GFP}$* for 10 s was carried out in the absence of Mg^{2+} and Ca^{2+} to avoid endocytosis of the label, which would lead to accidental observation of internalized vesicles (c.f. Hoopmann et al., 2010). Additionally, I added one condition in which I applied a 600 AP stimulation train, also followed by labelling and fixation. Figure 2.3 shows a summary of all experimental conditions, as well as controls.

condition	surface block	stimulation	recovery	labelling
un-blocked	-	-	-	+
resting	+	-	-	+
200 AP - 0 s	+	200 AP	-	+
200 AP - 30 s	+	200 AP	30 s	+
200 AP - 60 s	+	200 AP	60 s	+
600 AP	+	600 AP	-	+

Figure 2.3 . Experimental conditions. Samples were either directly labelled with $sdAb_{GFP}$* after incubation with $sdAb_{GFP}$ or mock incubation with Tyrode ("un-blocked" and "resting" conditions), or subjected to different stimulation paradigms after blocking (conditions termed "200 AP", "200 AP 30 s", "200 AP 60 s", "600 AP"). **Surface block:** Hippocampal neuronal cultures expressing sypHy or spH were incubated for 5 minutes with 175 nM $sdAb_{GFP}$. **Stimulation**: Cultures were electrically stimulated with 20 Hz pulses for 10 s (200 action potentials, AP) or 30 s (600 AP), followed by an optional **recovery** phase of 30 s or 60 s. **Labelling:** $sdAb_{GFP}$* was applied for 10 s, cultures were briefly washed and rapidly fixed in ice-cold fixative.

2.2 Tracking of newly exocytosed vesicles in synaptophysin-pHluorin expressing neurons

After having established the experimental protocol for the tracking assay, I proceeded to perform the assay on neurons expressing synaptophysin-pHluorin (sypHy).

STED microscopy succeeds in visualizing vesicles labelled by the tracking assay

In Figure 2.4, exemplary images of synaptic boutons expressing sypHy are presented for the different experimental conditions described in Figure 2.3. To establish the locations of transfected synaptic boutons, sypHy was imaged in confocal. $SdAb_{GFP}$* fluorescence was visualized with STED microscopy. The surface of the un-blocked sample is predominantly too densely labelled to allow for distinguishing single vesicles. The resting condition shows only background noise in the $sdAb_{GFP}$* channel, thereby confirming that $sdAb_{GFP}$ occupies all surface-resident GFP molecules. In all stimulation conditions, the labelling of newly available

GFP epitopes by $sdAb_{GFP}$* results in a clear punctate/spot pattern visible on the surface of the synaptic boutons.

Size and fluorescence intensity of the revealed spots can be determined by image processing

Synaptic vesicles can be approximated as circles/concentric fluorescent spots, which image processing methods can recognize and describe fairly easily. The location of the spots is found by identifying local maxima in fluorescence intensity. Lorentzian fits to line scans through the spots then provide information about the size (full-width at half-maximum of the fitted curves; FWHM) and peak fluorescence intensity of the spots (c.f. Figure 2.5 A). The FWHM is a more robust measure for the size of a spot than the width of the base of the fitted curve. However, it needs to be kept in mind that the FWHM will slightly underestimate the actual spot size.

Changes in peak intensity and size in the time course after stimulation are indicative of the fate of synaptic vesicles upon fusion

The most stringent information that the nanobody-based tracking assay provides about the fate of synaptic vesicles upon fusion is the development of peak intensity and FWHM of the identified spots in the time course of recovery after stimulation, i.e. the comparison of these parameters in the conditions 200 AP – 0 s, 30 s and 60 s. Two changes are to be expected to occur over time in the case that vesicles lose their integrity upon fusion with the cell membrane: 1) The frequency of observing spots that are slightly larger than expected for a fully collapsed

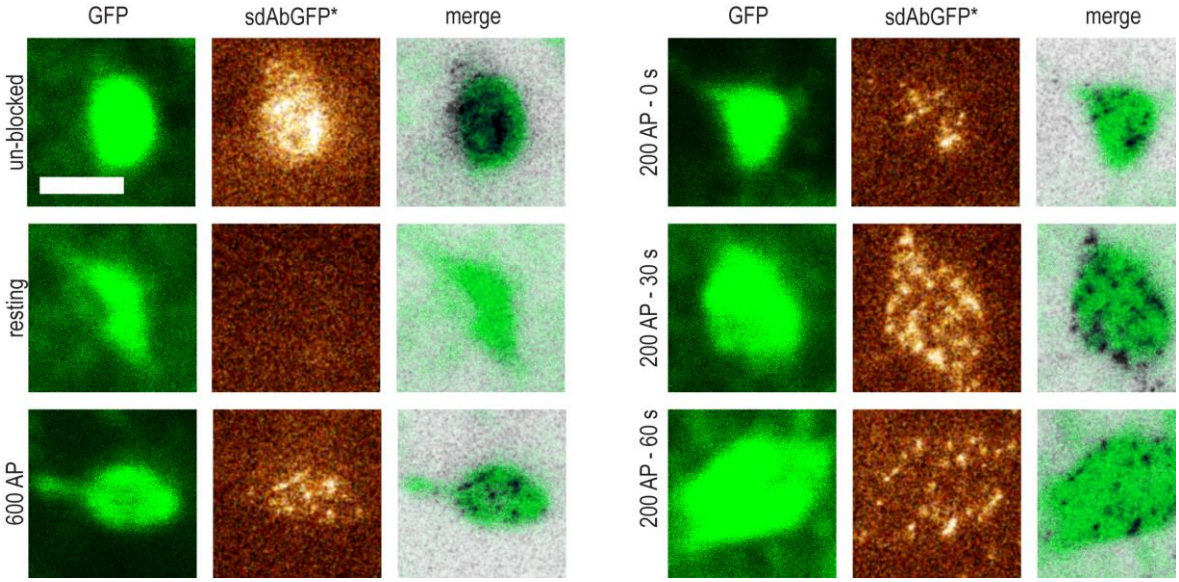

Figure 2.4 Visualization of newly exocytosed vesicles in sypHy expressing neurons. Neuronal cultures transfected with sypHy were incubated for 5 min at 37°C with $sdAb_{GFP}$ in divalent-free Tyrode, followed by optional stimulation in standard Tyrode solution and labelling with $sdAb_{GFP}$* (for a detailed description of the conditions refer to Figure 3.2). After labelling, samples were briefly washed with divalent-free Tyrode, and transferred to ice cold fixative solution containing 4% PFA and 0.2 % glutaraldehyde. Left panels: GFP signal in confocal, middle panels: STED images of $sdAb_{GFP}$-Atto. Right panels: merge. For easier viewing, STED images are presented after application of a 1 px gaussian blur, and merged images were additionally inverted. Scale bar 1 µm.

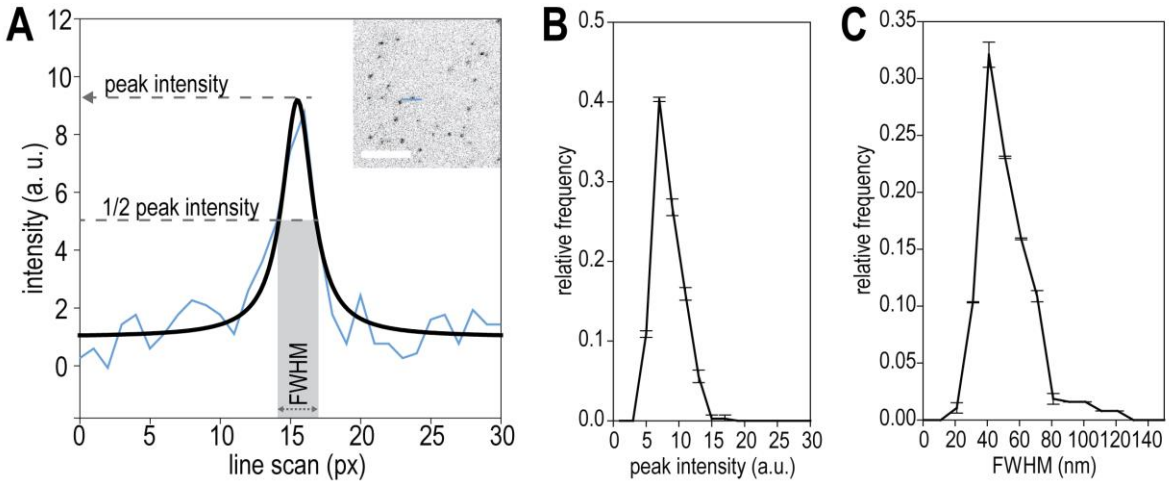

Figure 2.5 Image analysis. A) Spot parameters. To evaluate the size and brightness of fluorescent spots, Lorentzian fits were performed on line scans, and the peak intensity and full-width at half-maximum (FWHM, a measure for the size of the spot) were determined. Blue line: line scan as indicated by the same color in the inset. Black: corresponding Lorentzian fit. Inset shows an example STED image of diluted sdAb$_{GFP}$* (3.5 nM) spotted on a coverslip. Scale bar 1 µm. **B) Peak intensity** and **C) FWHM of sdAb$_{GFP}$* spots.** Histograms show distribution of peak intensity and FWHM of fluorescent spots in STED images of sdAb$_{GFP}$* spotted onto coverslips. Values are mean +- SD of 377 spots from two independent experiments. Histogram bins: 10 nm (FWHM) and 2 a.u. (peak intensity)

vesicle on the plasma membrane would increase, as vesicles would lose cohesion and drift apart and 2) at the same time the relative amount of spots that are small dim would also increase, due to the vesicles completely disintegrating and proteins diffusing freely over the plasma membrane, which would result in the detection of single vesicle proteins.

Single sdAb$_{GFP}$ molecules can be detected with STED microscopy*

To assess whether the STED setup I am using is able to detect fluorescence originating from single sdAb$_{GFP}$* molecules, I fixed highly diluted sdAb$_{GFP}$* onto a glass coverslip and acquired STED images of the sample. As evident from the image in the inset of Figure 2.5 A, fluorescent spots can be clearly detected. Analysis of the peak intensity and FWHM reveal a fairly homogenous, dim population of spots with an apparent FWHM of 20 to 80 nm (Figure 2.5 B, C). The small amounts of larger spots can be accounted for by coincidental colocalization or aggregation of sdAb$_{GFP}$* molecules. For further analysis, and comparison with experimental conditions of the tracking assay, spots > 80 nm were excluded from this set of data, which will from here on be referred to as “single molecules”.

Spot intensity and FWHM of structures labelled vary greatly and show no immediately discernible pattern according to experimental conditions

Figure 2.6 A presents an overview of the FWHM and peak intensity distributions of sdAb$_{GFP}$* spots identified in sypHy expressing neurons that were exposed to the different experimental paradigms of the tracking assay. Peak intensities vary between 5 and 400 arbitrary units (a.u.),

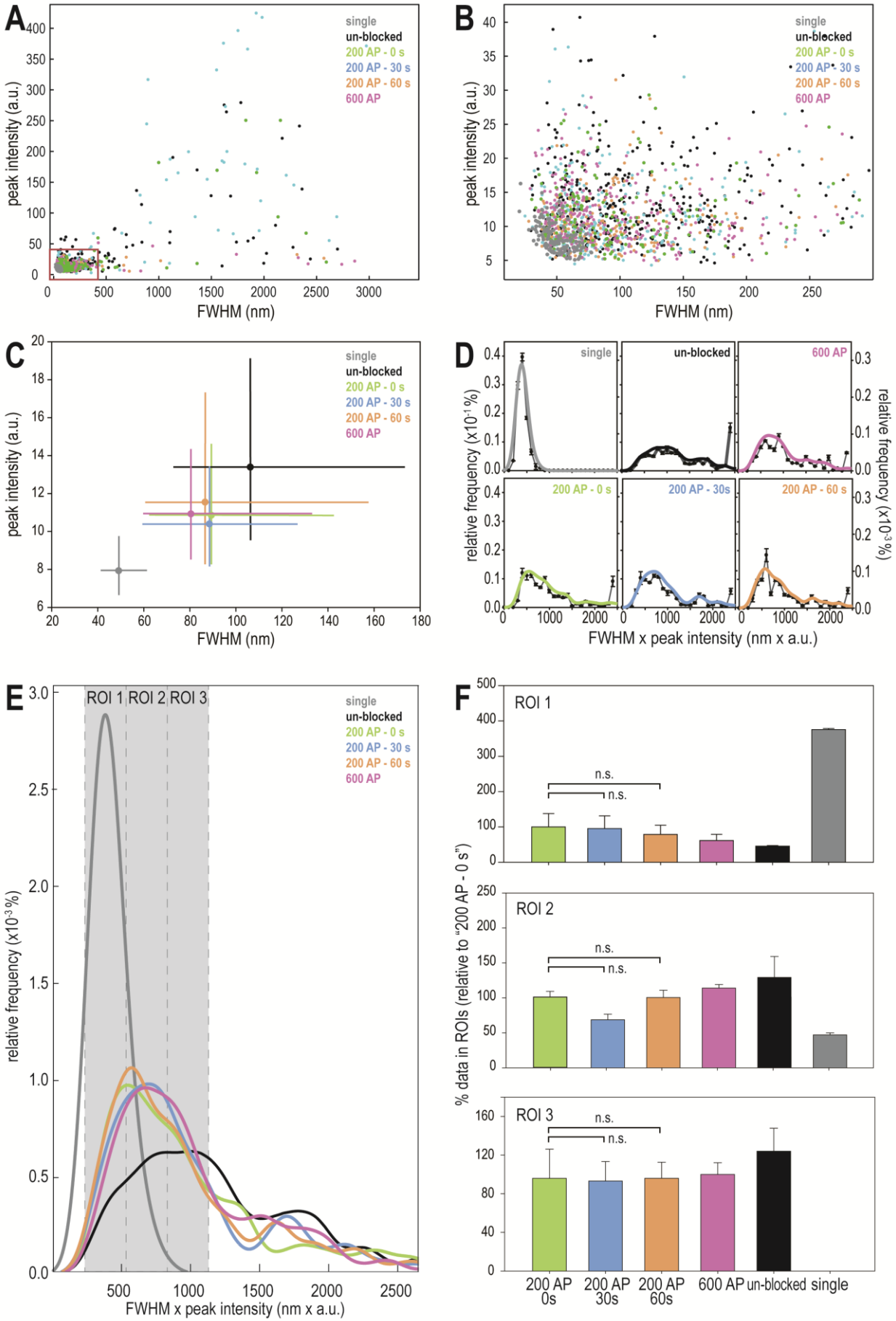

Figure 2.6 Parameters of newly exocytosed vesicles in neurons expressing sypHy. Caption continued on following page.

and FWHM between 20 and 3000 nm, with most of the data appearing to be clustered in the 5 to 40 a.u. and 20 to 300 nm range. The very large spots represent clusters of vesicles in which single vesicles cannot be distinguished. With the present assay, it cannot be determined whether the vesicles inside these clusters have intermixed or whether their proximity to each other is merely smaller than the resolution limit of STED microscopy. I therefore applied an arbitrary cutoff of 300 nm to my data before proceeding to further analysis. Figure 2.6 B shows an overview of this new limited dataset. As is to be expected, the values of the dim and small single molecule subset of data cluster in the lower left corner of the plot, whereas the un-blocked sample seems to contain slightly more large and bright spots than the rest of the data. This observation is confirmed when looking at the median and 25^{th}/75^{th} percentiles of the datasets (Figure 2.6 C): The median of the single molecule dataset is separate from the medians of the stimulated conditions, which are similar to each other. The un-blocked sample contains more larger and brighter spots.

The product of FWHM and peak intensity is an overall indicator for the size of vesicles observed

Spot size and peak intensity are by their nature positively correlated – increases in size and intensity are both the result of more $sdAb_{GFP}$* molecules, which contain exactly one fluorophore each, being present in the respective spot. Potential differences between the experimental conditions of the tracking assay should therefore become more easily discernible when considering the product of FWHM and peak intensity, instead of the separate factors. Figure 2.6 D shows histograms of the distribution of the product of FWHM and peak intensity (from here on referred to as "FWHM*peak") for all experimental conditions and controls. To be able to visually compare the histograms more easily, I fitted probability distribution functions (pdfs, Figure 2.6 D, continuous lines) and plotted them into one graph (Figure 2.6 E). In accordance

Figure 2.6. (previous page) Parameters of newly exocytosed vesicles in neurons expressing sypHy. A) Size vs peak intensity of $sdAb_{GFP}$* fluorescent spots, and **B) Closeup of the region indicated by the red rectangle in A.** Experimental conditions and analysis of parameters as described in **Figure 2.3** and **2.4.** N ≥ 193 spots per condition from 3 replicates with ≥ 5 synapses analysed each. **C) Correlation of FWHM and peak intensity in the area of interest.** Data are mean +- the 75^{th} and 25^{th} quantile respectively. **D) Relative frequencies of the product of FWHM and peak intensity in the different experimental conditions.** Histograms (left y axis) show mean +- SEM from 3 replicates. Bin size = 100. Probability distribution functions (right y axis) were fit to the histograms by a kernel density estimate using an unbounded kernel with bandwidth 100. **E) Regions of interest.** Coloured lines represent probability distributions for all conditions as in D. Three regions of interest (grey boxes) were defined. ROI1: 380 - 680 (determined by the peak of the single molecule probability distribution function +- 150). ROI2: 680-980. ROI3: 980-1280. **F) Percentage of data points in each ROI.** Graphs show mean +- SEM from 3 replicates each, normalized to the "200 AP" condition.

Grey: single molecules. Green: 200 AP - 0s. Blue: 200 AP – 30 s. Orange: 200 AP – 60 s. Magenta: 600 AP. Black: un-blocked.

with the previous figures, the most notable differences that can be seen are between the single molecule dataset, the stimulated conditions and the un-blocked conditions. As mentioned before, the most robust indicator for vesicles losing their integrity during their time in the surface pool would be an increase of the relative amount of small and dim spots, corresponding to single molecules being lost from disintegrating vesicles, in the 200 AP – 30 s and 200 AP – 60 s conditions compared to the 200 AP – 0 s condition. I used the pdf fitted to the single molecule dataset to define three regions of interest (ROI): ROI1 is centered on the maximum of the single molecule pdf and its half width is determined by the x position at half maximum of the left tail of the function. ROI2 and ROI3 were generated by moving ROI1 to the right by its width and twice its width respectively. Notably, the pdf of the un-blocked sample appears to have local maxima that fall into the ROIs, possibly indicating vesicles labelled by one, two, and three $sdAb_{GFP}$* molecules each.

The frequency of single molecule spots observed in sypHy expressing neurons does not change in the time course after stimulation

After having defined ROIs based on pdfs fitted to the data, I returned to the original dataset to determine the relative amounts of spots falling into these ROIs in the different experimental conditions, and compared these amounts to those in the 200 AP – 0s condition (Figure 2.6 F). There appears to be a tendency for the amounts of spots falling into ROI1 to decrease and the amounts of spots falling into ROI2 to increase over the course of recovery after stimulation; however, none of these differences are statistically significant. The same holds true for ROI3. The 600 AP condition exhibits FWHM*peak values similar to the other stimulated conditions.

2.3 Tracking of newly exocytosed vesicles in synaptobrevin-pHluorin expressing neurons

In addition to sypHy-expressing neurons, I also applied the nanobody-based tracking assay to neurons expressing synaptobrevin-pHluorin (spH).

Newly exocytosed vesicles can also be visualized in spH expressing neurons

Figure 2.7 shows representative images of spH expressing neuron subjected to the different tracking assay conditions spH. Note that, as previously described, the spH construct localizes not only to synaptic boutons, but also to the intersynaptic axonal segments. Similarly to the corresponding images for sypHy expressing neurons, a dense surface labelling with $sdAb_{GFP}$* can be observed in the un-blocked condition, whereas the blocked condition shows complete absence of $sdAb_{GFP}$* fluorescence. The stimulated conditions exhibit a punctate pattern, confirming that newly exocytosed vesicles are also successfully labelled in spH expressing neurons. Interestingly, labelling can also be observed in the axonal segments not only of the unblocked condition, but also of the stimulated conditions, even shortly after the stimulation event. This is in accordance with the findings of Fernández-Alfonso et al. 2006, who observed

rapid diffusion of newly exocytosed spH into axonal segments after stimulation. Additionally, synaptobrevin in general localizes to synaptic vesicles more poorly than synaptophysin, which implies it can be more easily lost into axons (Rizzoli 2014). To assess whether newly

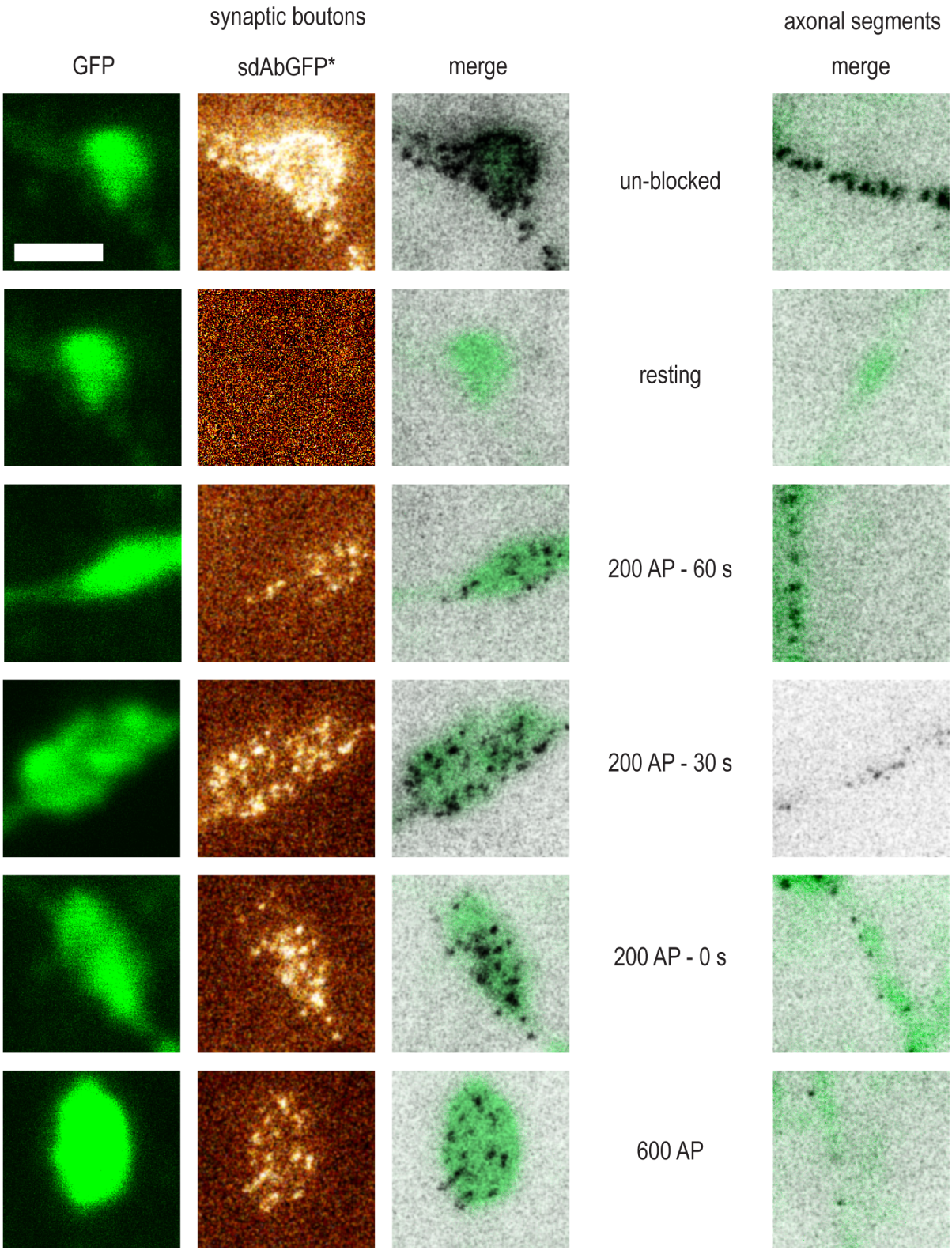

Figure 2.7 Visualization of newly exocytosed vesicles in synaptic boutons and axonal segments of spH expressing neurons. Conditions and image processing as in Figure 2.6

exocytosed spH molecules suffer a different fate in the axonal segments than in synaptic boutons, I analysed fluorescent spots identified in these two areas separately.

The relative amount of small and dim spots stays constant in synaptic boutons of spH expressing neurons in the time course of recovery, but increases in axonal segments

Figures 2.8 A-D show scatter plots of single spots as well as median and 25^{th}/75^{th} percentile of FWHM and peak intensity in the different assay conditions in synaptic boutons (Figures 2.8 A, C), and axonal segments (Figures 2.8 B, D). While the values for synaptic boutons present relatively similar to those in sypHy expressing neurons, the distributions of the fluorescent spots detected in axons show marked differences. Overall, there appear to be less large and bright spots, which is consistent with the fact that the axonal surface is smaller per se. Figure 2.8 D, however, shows that for axons there is an appreciable overlap of stimulated conditions with the single molecule dataset. Furthermore, the median value for FWHM and peak intensity appears to shift towards the lower left corner of the graph over the course of recovery after stimulation (200 AP – 0 s, 30 s, and 60 s conditions). To assess whether this observation represents a significant change, I again fitted probability density functions to the histograms of FWHM*peak (Figures 2.8 E, F), and applied the same ROIs as for sypHy expressing neurons (Figures 2.8 G, H). Visually, the impression that the proportion of small and dim spots present in axonal segments increases during recovery, but stays relatively constant in synaptic boutons, is confirmed. Figure 2.8 I reveals that indeed the relative amounts of spots compared to the 200 AP – 0 s condition does not significantly change in the 60 s time course after stimulation for any of the ROIs. By contrast, in axonal segments, the amounts of small and dim spots (ROI1) significantly increases in the 200 AP – 60 s condition compared to 200 AP – 0s ($p=0.05$; Figure 2.8 J). Conversely, there is also a significant decrease ($p=0.05$) in the amounts of spots falling into ROI2 between the 200 AP – 0 s and 200 AP – 60 s conditions. In the 600 AP condition, more large and bright spots appear to be present in axonal segments, which suggests that due to the harsh stimulation and limited space labelled spH proteins are more likely to be in too close proximity to be separated by STED microscopy.

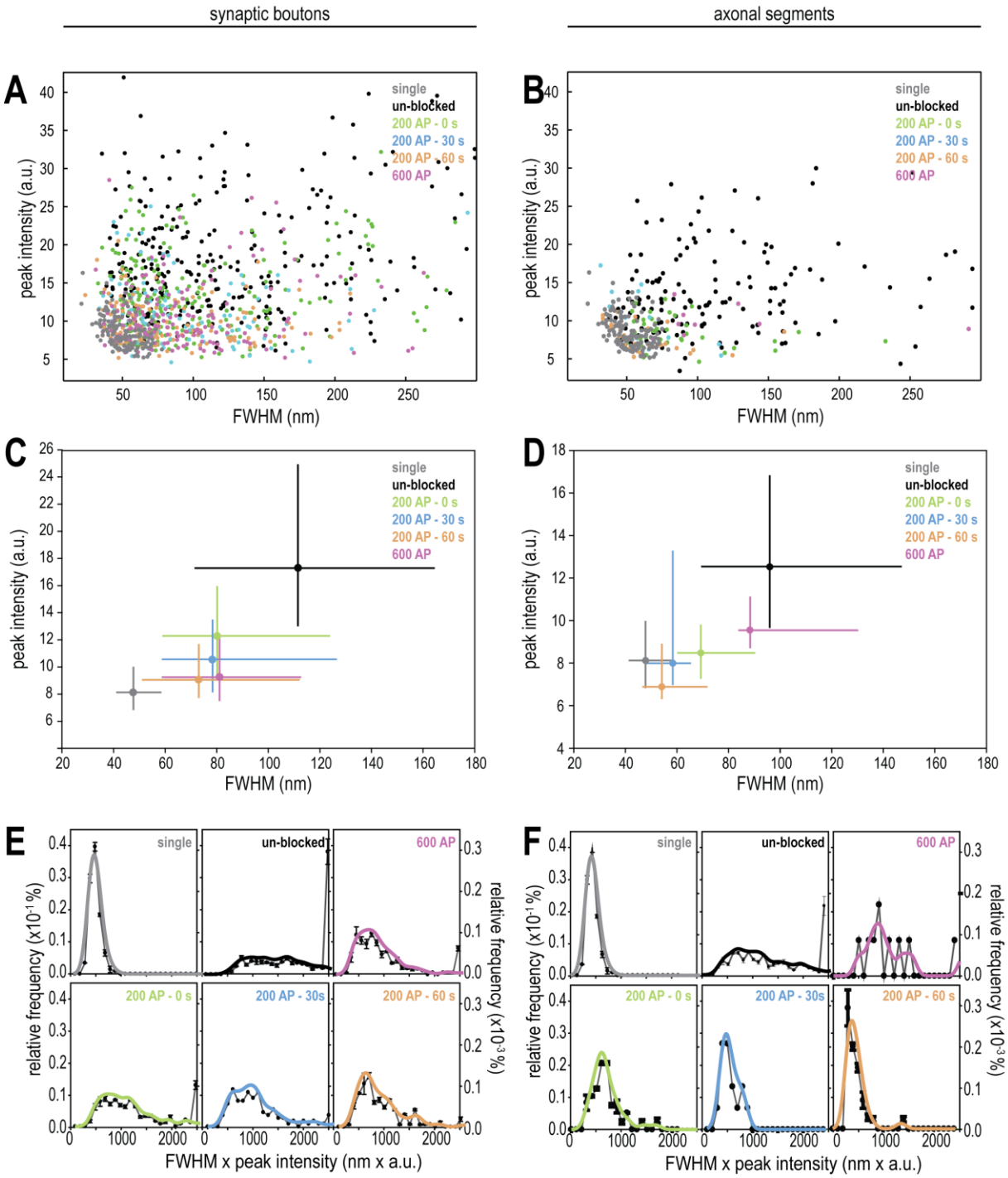

Figure 2.8 Parameters of newly exocytosed vesicles in neurons expressing spH. A, B) Size vs peak intensity of sdAb$_{GFP}$* fluorescent spots. N ≥ 119 spots (synaptic boutons) and N ≥ 40 spots (axonal segments) per condition from 2 replicates with ≥ 5 areas analysed each. **C, D) Correlation of FWHM and peak intensity.** Data are mean +- the 75th and 25th quantile respectively. **E, F) Relative frequencies of the product of FWHM and peak intensity in the different experimental conditions.** Histograms (left y axis) show mean +- SEM from 2 replicates. Bin size = 100. Probability distribution functions (right y axis) were fit to the histograms by a Kernel density estimate using an unbounded kernel with bandwidth 100. **G, H) Regions of interest.** Coloured lines correspond to the probability distribution functions fitted in E and F. ROIs were defined as in Figure 2.6. **I, J) Percentage of data points in regions of interest.** Graphs show means +- SEM from 2 replicates each (except 200 AP – 30 s and 600 AP conditions with n=1), normalized to the "200 AP" condition. * indicates p≤0.05 according to Student's t-test.

Grey: single molecules. Green: 200 AP - 0s. Blue: 200 AP – 30 s. Orange: 200 AP – 60 s. Magenta: 600 AP. Black: un-blocked.

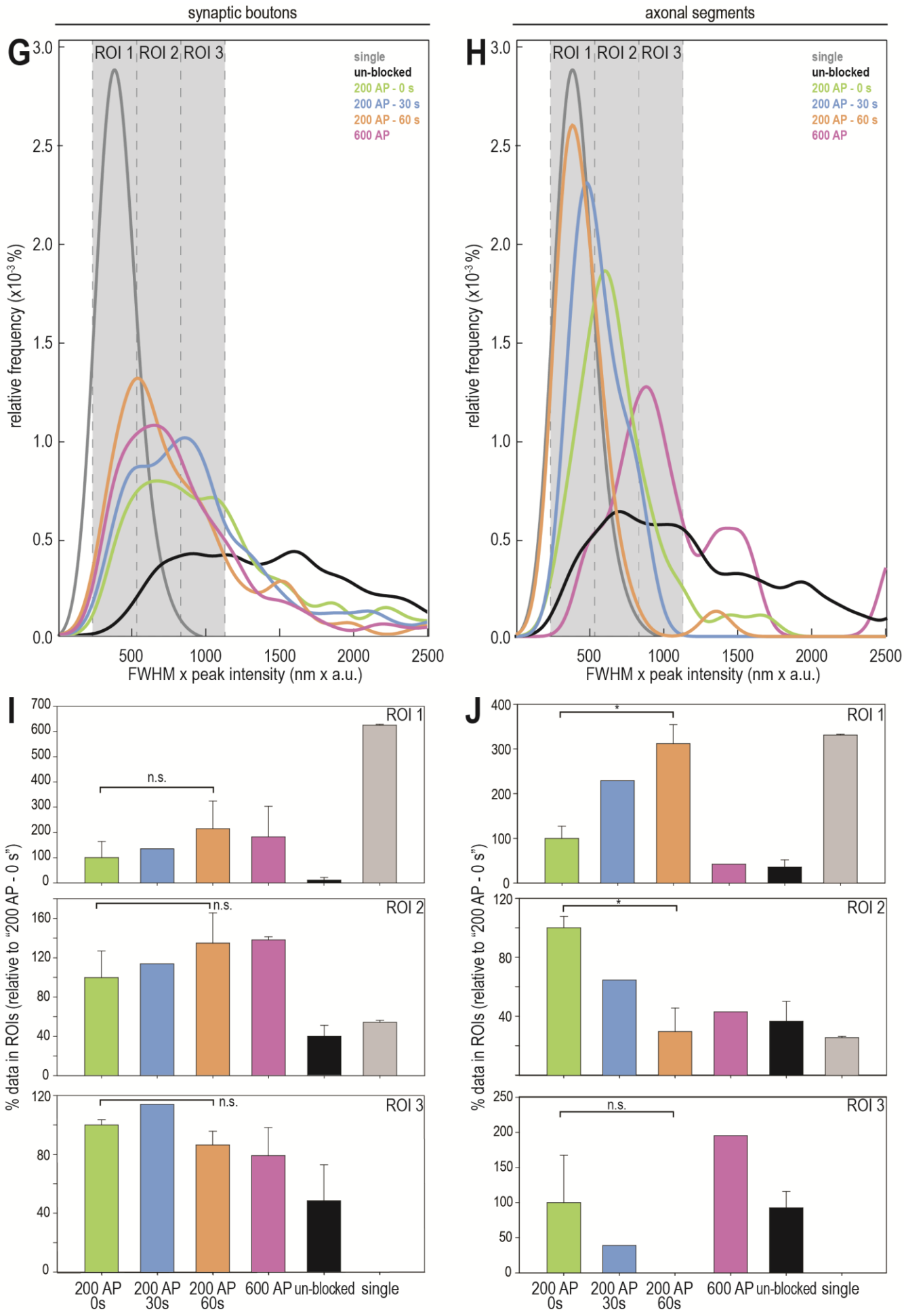

Figure 2.8 (continued)

2.4 Tracking of newly exocytosed vesicles in *Drosophila melanogaster* larval neuromuscular junctions

To demonstrate the transferability of the tracking assay to other model systems, I also carried it out on *Drosophila melanogaster* larval neuromuscular junction (dNMJ) preparations.

Blocking of surface epitopes by sdAb$_{GFP}$ is also efficient in dNMJs

First, I confirmed that sdAb$_{GFP}$ also succeeds in blocking surface-resident GFP epitopes in dNMJ preparations of *Drosophila* larva panneuronally expressing synaptobrevin-pHluorin. Figure 2.9 demonstrates that application of 350 nM sdAb$_{GFP}$ results in complete inhibition of subsequent sdAb$_{GFP}$* binding. At 35 nM concentration, enough GFP epitopes remain un-blocked for a clear sdAb$_{GFP}$* labelling to be visible. Therefore, for future experiments, I used 350 nM sdAb$_{GFP}$ for blocking.

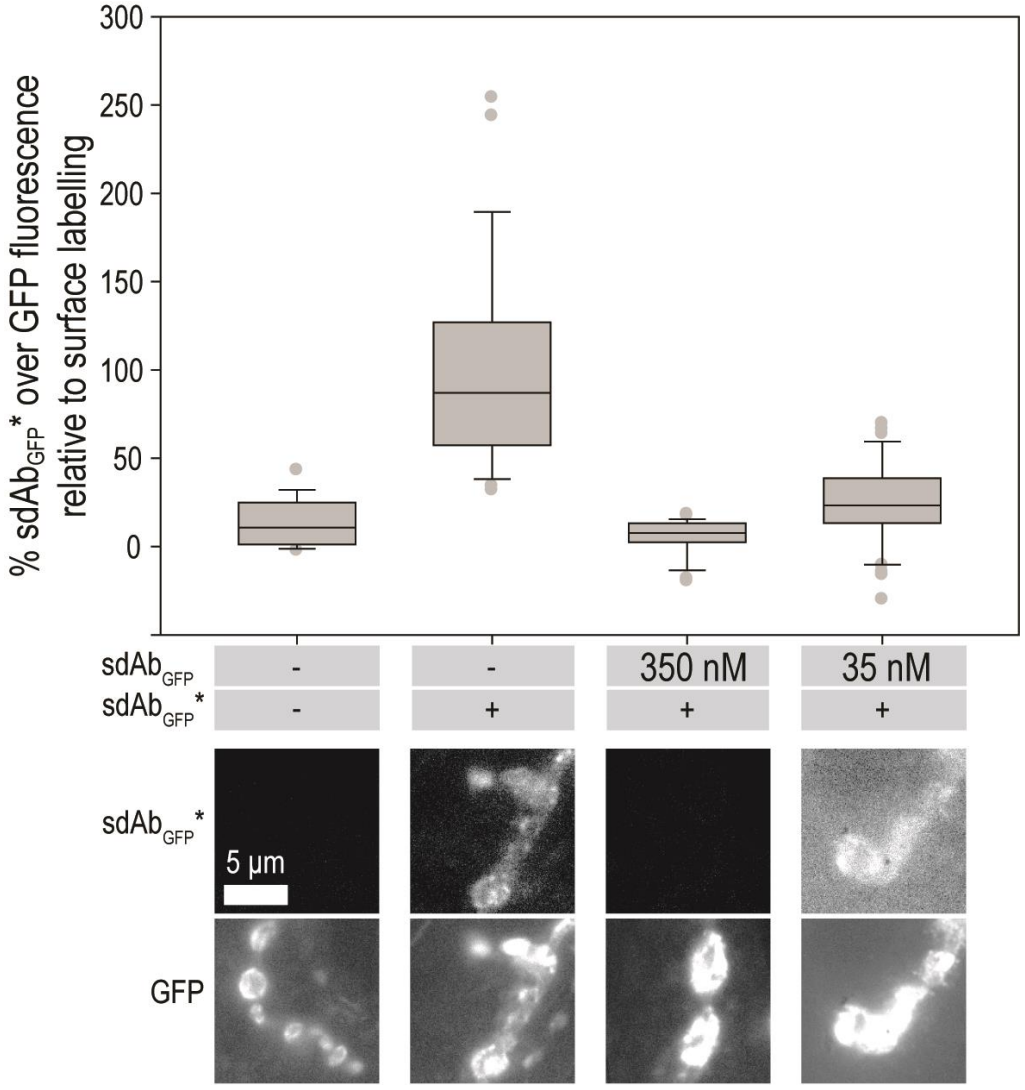

Figure 2.9 Blocking of surface-resident GFP epitopes of dNMJs expressing spH. Preparations were incubated with sdAb$_{GFP}$ for 5 min at the concentrations indicated, washed briefly, and stained with sdAb$_{GFP}$* for 2 minutes. Y-axes indicate the ratios of sdAb$_{GFP}$* fluorescence over GFP fluorescence in synaptic boutons, relative to complete surface labelling. N ≥15 synapses each. Epifluorescence images, scale bar 5 µm.

Super-resolution imaging of dNMJ preparations can be achieved by embedding and thin sectioning

Acquiring super-resolution images in tissue samples is not trivial due to spherical aberrations and the diffraction-limited z-resolution of the technique. When trying to image dNMJ preparations of spH expressing larva that were live stained with $sdAb_{GFP}$* (i.e. the unblocked condition), I encountered this problem. With conventional Mowiol mounting of the samples, the

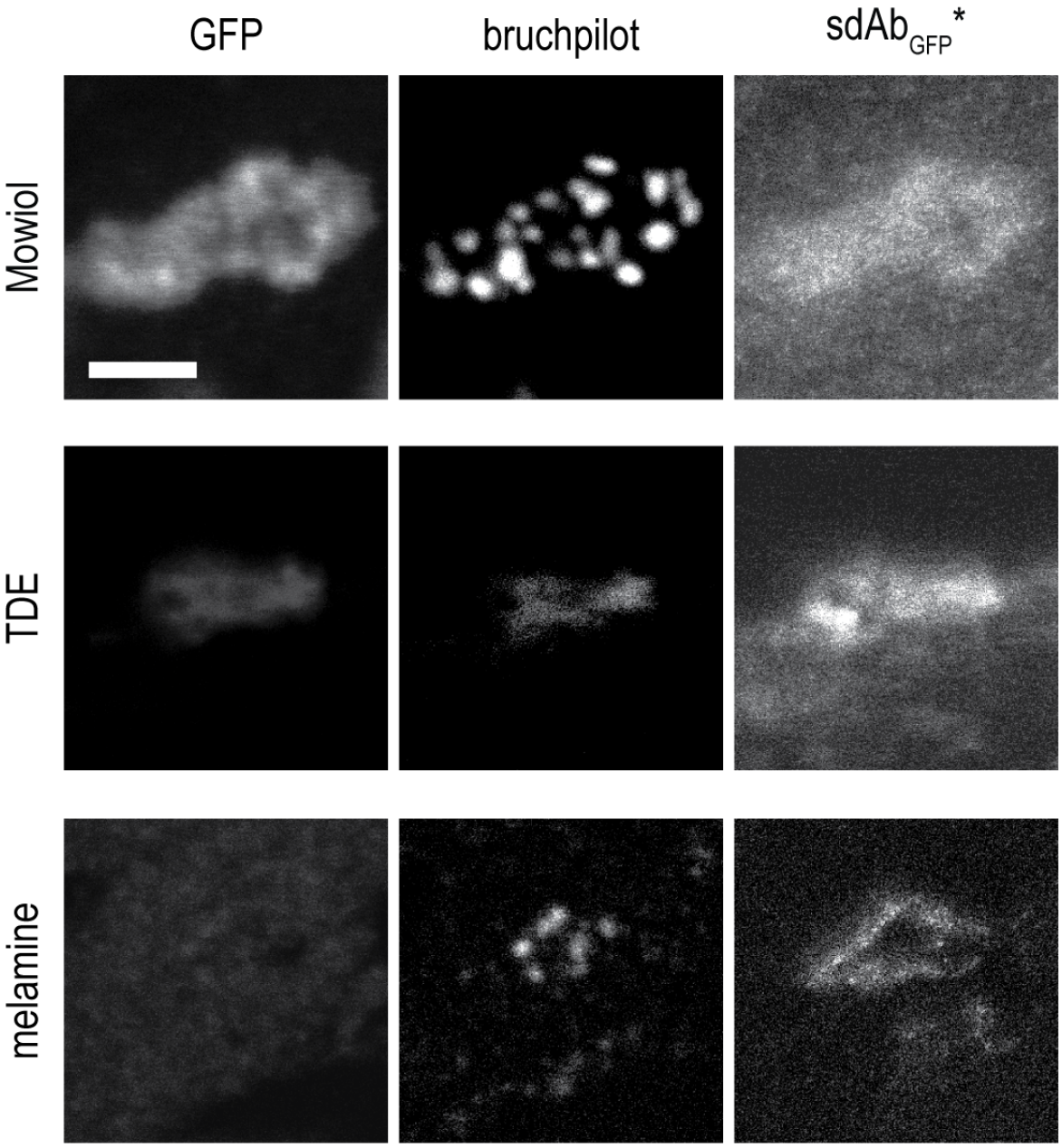

Figure 2.10 Super-resolution imaging of dNMJ preparations. Third instar *Drosophila* larval preparations expressing spH panneuronally were live stained with $sdAb_{GFP}$-Atto and subsequently fixed, permeabilized and immunostained with an antibody against bruchpilot and corresponding secondary antibody in the Cy3 channel. Samples were either mounted in Mowiol or thio-diethanol (TDE), or embedded in melamine and processed into 200 nm thin sections. GFP and bruchpilot in confocal, $sdAb_{GFP}$* in STED. Scale bar 2 µm.

resolution of the sdAb$_{GFP}$* signal is very poor (Figure 2.10). Therefore, I proceeded to perform mounting in thio-diethanol (TDE). During a series of incubations with increasing TDE concentrations, water in the sample is replaced by TDE, which has a refractive index equal to that of immersion oil. Thereby, diffraction at the sample – coverslip – immersion oil interfaces is minimized, resulting in reduced spherical aberrations and improving resolution. However, in my hands TDE embedding did not enable me to acquire super-resolution images of sdAb$_{GFP}$* labelled samples (Figure 2.9). Another measure to improve z-resolution in thick specimens is embedding them in a plastic resin, for example melamine, and processing into thin sections (e.g. 200 nm) using an ultramicrotome. In this way, I could acquire super-resolution images of sdAb$_{GFP}$* labelled dNMJs (Figure 2.9). Note that after melamine embedding, spH is no longer fluorescent, most likely due to the long incubation steps (several days) at high temperatures that are required for the procedure.

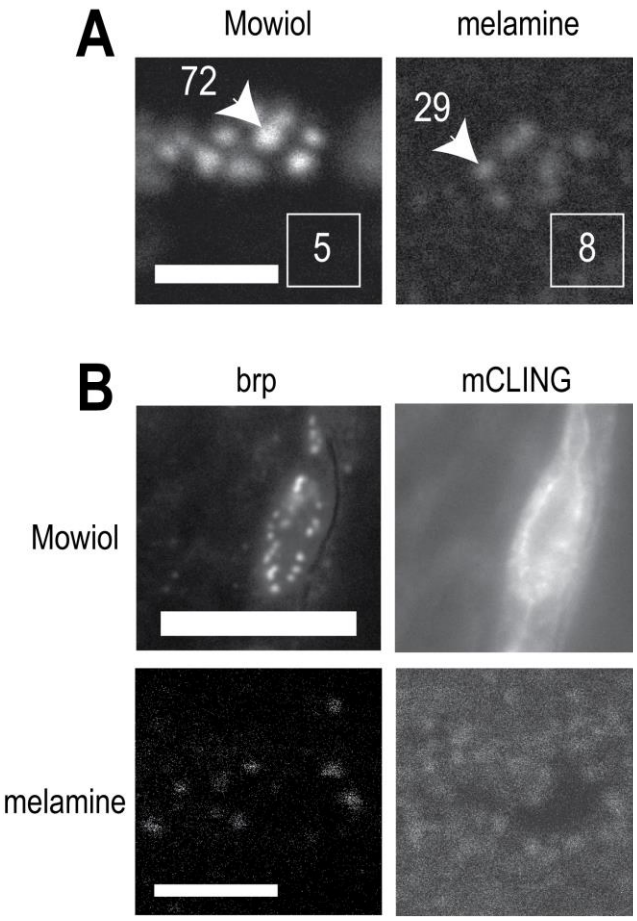

Figure 2.11 Fluorescence intensities in whole mounted *Drosophila* larval fillets compared to 200 nm ultrathin sections. A) Larval preparations were fixed and immunostained for bruchpilot with a Cy3 secondary antibody and either mounted in Mowiol or processed into ultrathin sections. Numbers next to arrows are mean fluorescence intensites (a. u.) in the spots indicated, numbers in squares indicated background fluorescence intensity in the area delineated by the squares. B) Membrane staining with mCLING-Atto488. Larval preparations were live stained with mCLING, fixed and immunostained for bruchpilot and either mounted in Mowiol or processed into ultrathin sections. Mowiol: epifluorescence images. Melamine: confocal images. Scale bars 2 µm.

Synaptic boutons are difficult to identify in thin sections of Drosophila larva preparations

Since GFP is no longer fluorescent after melamine embedding, other means need to be employed to identify areas with synaptic boutons for imaging in thin sections of *Drosophila* larva preparations. Aside from the fact that strong sdAb$_{GFP}$* fluorescence is not expected in all experimental conditions of my assay, it is at any rate not suitable for this purpose, as Atto647 fluoresces in the far-red spectrum and is almost invisible to the human eye. Boutons could potentially also be identified by immunolabelling of synaptic proteins, or by a general membrane staining. Unfortunately, thin

sectioning of fluorescently labelled samples inherently leads to reduced fluorescence intensity in the single sections compared to whole-mounted samples. Fluorescence from an immunostaining against the active zone protein bruchpilot is already quite dim in whole-mounted dNMJ preparations. In thin sections, the signal to noise ratio of fluorescence from a Cy3 secondary antibody against the bruchpilot antibody is even lower – by a factor of four in the example images shown in Figure 2.11 A – which renders the signal almost invisible to the eye when examining sections through the microscope eyepiece in epifluorescence illumination. Searching for boutons in scanning confocal mode, in addition to being impractical because of the lower speed and smaller field of vision, is also not an option, as when a stained region is identified, the signal is almost immediately lost again to photobleaching. The same issues hold true for an antibody immunostaining against GFP (not shown) and general membrane staining by the membrane dye mCLING (Figure 2.11 B). Summarizing, the only way in which I could find the positions of synaptic boutons in thin sections was by identifying possible regions by morphology, and attempting to make out the extremely dim fluorescent signals from immunostainings. Since this is a rather tedious and time-intensive process, I only investigated two conditions of the tracking assay with STED microscopy (un-blocked and 600 AP stimulation), as a proof of principle for the transferability to dNMJs.

Newly exocytosed vesicles can also be visualized in dNMJ preparations

Figure 2.12 A shows synaptic boutons of spH-expressing dNMJs treated according to the un-blocked and 600 AP experimental paradigms of the $sdAb_{GFP}$ tracking assay. As in neuronal cultures, a comprehensive surface labelling is observed in the unblocked conditions. SpH proteins that have been exocytosed in the course of a 600 AP stimulation course present as a clearly delineated punctate pattern. The FWHM and intensity distributions of fluorescent spots of the un-blocked condition are clearly distinct from those of single molecules (Figure 2.12 B), whereas a considerable proportion of spots labelled in the stimulation condition exhibit parameters matching those of single molecules (Figures 2.12 B and C).

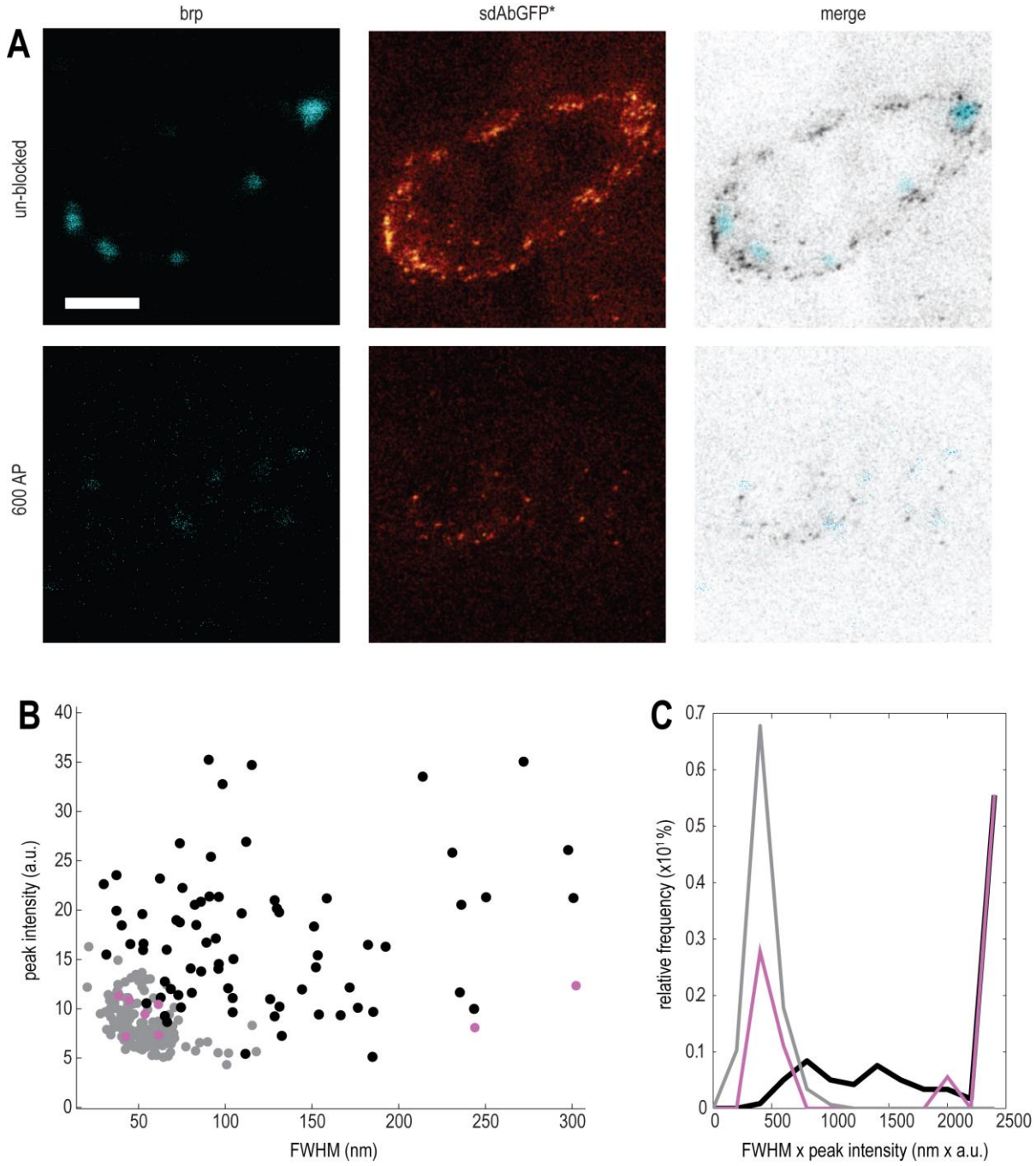

Figure 2.12 Visualization of newly exocytosed vesicles in dNMJ preparations. A) STED images of newly exocytosed vesicles. DNMJ preparations expressing spH were either surface-labelled with sdAb$_{GFP}$* (un-blocked) or blocked with sdAb$_{GFP}$ and labelled with sdAb$_{GFP}$* after a 600 AP electrical stimulation. Preparations were fixed, immunostained for the active zone protein bruchpilot, and processed into 200 nm sections after melamine embedding. Brp imaged in confocal, sdAb$_{GFP}$* in STED. Scale bar 3 µm. **B) FWHM and peak intensity of fluorescent spots** in the un-blocked condition (black), 600 AP conditions (magenta) and of single molecules (grey). **C) Histograms of the product of FWHM and peak intensity in the same conditions.** Bin size = 100. Colours as in B

3. DISCUSSION

In this work, I have shown that an sdAb against GFP can be successfully used in conjunction with STED microscopy to track newly exocytosed synaptic vesicles in hippocampal neuronal cultures as well as dNMJ preparations; that the amounts of apparently orphaned newly exocytosed sypHy and spH proteins present on the surface of synaptic boutons of neurons transfected with these proteins do not change during the first minute of recovery after electrical stimulation; and that by contrast the amount of single spH proteins present in the inter-bouton axonal segments of spH transfected neurons increases during the same time frame. Figure 3.1 shows a summary of these findings.

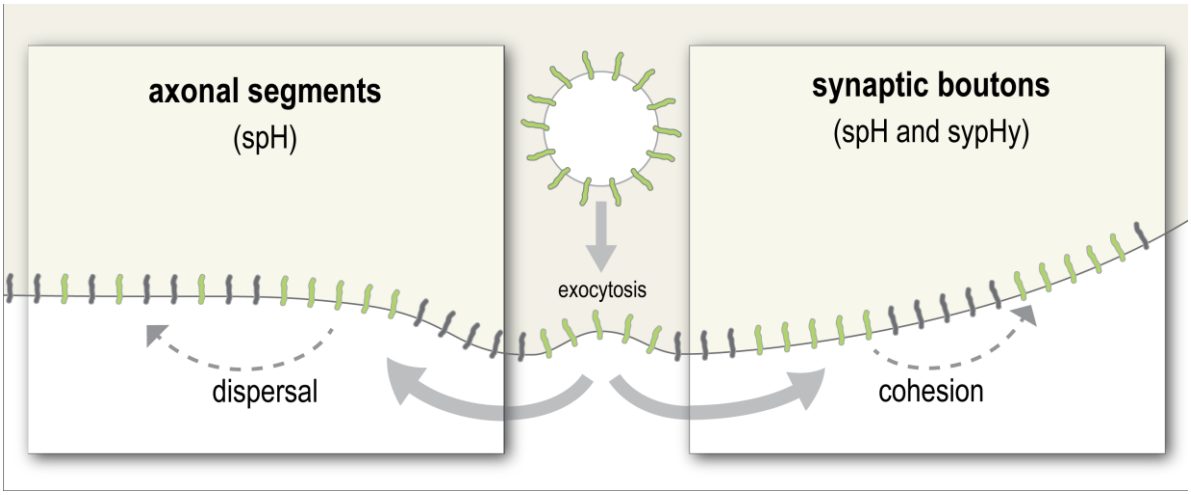

Figure 3.1. SpH and sypHy remain clustered on the surface of synaptic boutons, whereas patches of spH proteins disintegrate on axonal membrane segments.

3.1 Prescence of single spH and sypHy proteins on the surface of synaptic boutons in all conditions

The fractions of spots of newly exocytosed proteins labelled with $sdAb_{GFP}$* that are of the same size and FWHM as a control consisting of single $sdAb_{GFP}$* molecules are considerable in all experimental conditions. Merely the un-blocked control, in which all surface resident GFP moieties are labelled, presents with comparably few small and dim spots (Figures 2.4, 2.7). This is likely an artifact of the artificial expression of the fluorescent proteins. It has been estimated, that on average only 2.3 spH molecules and 3.1 sypHy molecules are targeted to each vesicle (Sinha 2011) - small amounts compared to the numbers of approximately 70 endogenous synaptobrevin and 31 endogenous synaptophysin molecules per vesicle, which are not accessible for labelling by $sdAb_{GFP}$* (Takamori et al. 2006; Wilhelm et al. 2014). The interspersal with endogenous proteins can potentially lead to pHluorins of the same vesicle to be as far apart as 90 nm (e.g. in the case of two pHluorin molecules being present at diametrally opposite positions of the vesicle protein patch of 90 nm diameter). Since the resolution limit of the STED microscope used in this work is approximately 50 nm, this could lead to the $sdAb_{GFP}$* labelled pHluorin molecules to be misidentified as separate vesicles.

Additionally, there is evidence for a considerable fraction of vesicles containing only a single pHluorin molecule (Balaji and Ryan 2007; Wienisch and Klingauf 2006).

Since, if the cohesion model applies, the relative amounts of those single pHluorin molecules mistakenly being identified as not being part of a synaptic vesicle should stay constant in all conditions due to the random nature of their occurrence, this phenomenon does not negatively affect the validity of the nanobody-based tracking assay. Significant increases in the number of single molecule spots over the time course of recovery after stimulation would still be indicative of loss of vesicle integrity.

3.2 Possible influences of GFP tagging on vesicle integrity

Opazo et al., 2010 found that sypHy and spH proteins are more diffusely distributed on the plasma membrane than their endogenous counterparts synaptophysin and synaptobrevin, which might suggest an inhibition of clustering by the pHluorin tag. If this were the case, conclusions drawn about the vesicle integrity problem that are derived from the analysis of pHluorin tagged proteins would not be very meaningful. However, the apparent diffuse distribution of pHluorins in the study of Opazo et al. can likely be accounted for by the aforementioned stochiometry of tagged to endogenous proteins, as well as by their use of antibodies for labelling the molecules. On the one hand, differences in affinity to their respective epitopes could lead to considerable differences in the quality of the immunostainings performed with the GFP antibody and ones performed with the antibodies against synaptophysin and synaptobrevin; a lower affinity might easily account for a more diffuse staining pattern. On the other hand, the issues described in 3.1 become even more exacerbated by the displacement of the observed fluorophores from their target, which could lead to even more pHluorins that are present in clusters being misidentified as non-clustered.

Furthermore, a study dedicated to investigating the clustering behavior of native and GFP-tagged proteins found no differences in clustering of native synaptobrevin and synaptophysin and their tagged counterparts (Vreja et al. 2015).

In conclusion, findings generated by the analysis of pHluorin tagged proteins can be assumed to be transferrable to native proteins.

3.3 Technical limitations

It needs to be acknowledged that the 200 AP – 0 s condition does not represent a true “time zero” after vesicle exocytosis. Due to the labelling time of 10 s, the vesicles exocytosed closest to the time point of observation (fixation) will already have been resident on the plasma membrane for 10 s. A possibility to circumvent this problem would be to apply $sdAb_{GFP}$* during stimulation. However, this could lead to endocytosis of the label and unintended observation of internalized vesicles, which would also distort the results. Alternatively, one could transfer

the samples to fixative immediately after stimulation, and apply $sdAb_{GFP}$* to the fixed samples. Fixation may however alter the GFP epitope, resulting in different affinity of $sdAb_{GFP}$*. To achieve the highest labelling density possible, which is essential for correctly determining the physical parameters of newly exocytosed vesicles, applying the probe to unfixed samples is preferable. Therefore, although it seems highly unlikely, I cannot completely exclude the possibility of vesicles completely disintegrating and reintegrating into different clusters within in the first 10 s after exocytosis.

3.4 A possible mechanism for the maintenance of synaptic vesicle integrity

I show that the number of newly exocytosed spH and sypHy molecules that are not in close proximity to other spH and sypHy molecules stays constant over the course of recovery after stimulation for proteins that remain on the surface of synaptic boutons (Figures 2.6 and 2.8). From this, I conclude that clusters of these proteins do not disintegrate over time, supporting the cohesion model of vesicle integrity. For spH molecules diffusing into interbouton axonal spaces after exocytosis, a marked difference can be observed over time in the relative amounts of proteins being present in clusters and those being present as single molecules. The amounts of single molecules (defined as those that fall into ROI1) present on axonal segments increases significantly in the first minute after stimulation, by 300 percent compared to the time immediately after stimulation, whereas the amounts of spots containing clustered molecules (with size and intensity profiles corresponding to ROI2) decrease significantly, to 35% of the original amounts (Figure 2.8. J). This implies that newly exocytosed vesicles diffuse into the axonal segments in patches and the patches lose their integrity in the time course of recovery after stimulation.

The escape of surface-resident vesicle material into axonal segments has been described mainly as a result of unphysiologically high stimulation intensities (Opazo et al. 2010), or as a property of overexpressed fusion constructs – the latter being the case with spH (Wienisch and Klingauf 2006). Although resulting from a rather artificial basis, the disintegration of spH-containing vesicles on the plasma membranes of axonal segments points to the mechanism by which vesicle integrity is maintained being based on a process that is likely to occur in synaptic boutons and not in axonal segments, as opposed to a mechanism inherent to the synaptic vesicle itself.

A likely candidate for such a process would be the assembly of endocytic proteins. Haucke et al. in 2011 proposed that exocytic-endocytic coupling is mediated by proteins of the cytoplasmatic matrix of the active zone, as well as scaffolds of endocytic proteins. These scaffolds may prevent the disintegration of synaptic vesicles after fusion. As shown by Denker et al. in 2011, soluble proteins involved in vesicle recycling, including those involved in endocytosis, are buffered by synaptic vesicles, most likely in order to maintain high enough local concentrations of these proteins where they are needed – in the synaptic boutons. Since

protein-protein interactions are not purposeful all-or-nothing binding events, but underlie a constant on-off-kinetic determined by local concentrations of the binding partners, the following model is conceivable to explain the disintegration of vesicles on axonal segments: After exocytosis, endocytic scaffolds start to assemble at the vesicle, leading to it briefly maintaining its integrity. However, upon diffusion into the axonal segments, the local concentrations of endocytic proteins and adapter proteins are lower and don't allow for the maintenance of the endocytic scaffolds. Consequently, vesicle integrity is lost.

3.5 Outlook

I have presented here an assay that can be easily adapted to different model systems and proteins. Any synaptic vesicle protein with an intravesicular domain that can be fused to GFP can be investigated in any model organism capable of exogenous expression of these GFP constructs. As soon as sdAbs specific for the luminal domains of vesicle proteins become available, the latter restriction is eliminated.

In its present form, the assay can only answer the question of whether vesicle proteins stay clustered during their time on the plasma membrane, or not. The possibility of vesicle components intermixing at other steps of vesicle recycling, e.g. fusion to the endosome, remains open. To address this issue, newly exocytosed vesicles could be labelled with $sdAb_{GFP}$ molecules conjugated to different fluorophores during multiple rounds of labelling, and the degree of intermixing of the different fluorescent labels after different recovery periods could be assessed by multi-color super-resolution microscopy.

Multi-color super-resolution microscopy could also be employed to investigate the possible role of endocytic proteins in maintaining vesicle identity. This would involve determining the degrees of colocalization of newly exocytosed vesicle proteins with different proteins of the endocytic machinery in the time course after exocytosis, as well as in synaptic boutons compared to axonal segments.

4. MATERIALS & METHODS

4.1 Probes

Probes used are listed in Table 1.

Table 1: Probes. Ab: antibody; **F_{ab}:** F_{ab} fragment; **sdAb:** single-domain antibody ("nanobody");

type	designation/target	fluorescent label	catalogue number	manufacturer	working dilution
Ab (mouse)	bruchpilot, *Drosophila melanogaster*	-	nc82	Drosophila studies hybridoma database (DSHB), Iowa, US*	1:25
Ab (mouse)	bassoon, *Rattus Norwegicus*	-	141 021	Synaptic Systems, Göttingen, Germany	1:100
Ab (mouse)	GFP	-	A11120	Invitrogen	1:20
F_{ab} (goat)	mouse	Cy3	115-167-003	Dianova, Terrebonne, QC, Canada	1:75
Ab (goat)	mouse	Alexa-488	A11011	Invitrogen, Carlsbad, CA, US	
sdAb	"FluoTag®-Q anti-GFP", GFP	-	N0300-1mg	NanoTag Biotechnologies GmbH, Göttingen, Germany	1:20
sdAb-Atto	"FluoTag®-Q anti-GFP", GFP	Atto647N	N0301-At647N-L	NanoTag Biotechnologies GmbH, Göttingen, Germany	1:100
membrane dye	mCLING	Atto488	710 006AT3	Synaptic Systems, Göttingen, Germany	1:400

*deposited to the DSHB by Buchner, E.

4.2 Chemicals

Chemicals used are listed in Table 2.

Table 2: Chemicals.

item	manufacturer
ammonium chloride	Merck KGaA, Darmstadt, Germany
BSA	Applichem, Darmstadt, Germany
$CaCl_2$	Sigma-Aldrich, St. Louis, MO, USA
DMEM	(Thermo Fisher Scientific, Waltham, MA, USA)
EpoFix Resin	Struers, Willich, Germany
Glucose	Merck KGaA, Darmstadt, Germany
glutaraldehyde	Sigma-Aldrich, St. Louis, MO, USA
Glycerol	Merck KGaA, Darmstadt, Germany
glycine	Merck KGaA, Darmstadt, Germany
HEPES	Merck KGaA, Darmstadt, Germany
KCl	Sigma-Aldrich, St. Louis, MO, USA
KH_2PO_4	Sigma-Aldrich, St. Louis, MO, USA
Melamine	TCI, Chiyoda, Tokyo, Japan
Mowiol	Merck KGaA, Darmstadt, Germany
Na_2HPO_4	Sigma-Aldrich, St. Louis, MO, USA
NaCl	Sigma-Aldrich, St. Louis, MO, USA
PFA	Sigma-Aldrich, St. Louis, MO, USA
p-tuloenesulfonic acid monohydrate	Sigma-Aldrich, St. Louis, MO, USA
thio-diethanol	Sigma-Aldrich, St. Louis, MO, USA
Triton-X 100	Sigma-Aldrich, St. Louis, MO, USA

4.3 Buffers/Solutions

PBS: 137 mM NaCl, 2.7 mM KCl, 10 mM Na_2HPO_4, 2 mM KH_2PO_4; pH 7.4

High-salt PBS: 500 mM NaCl, 2.7 mM KCl, 10 mM Na_2HPO_4, 2 mM KH_2PO_4; pH 7.4

Tyrode: 124 mM NaCl, 25 mM HEPES, 30 mM Glucose, 2 mM $CaCl_2$, 5 mM KCl, 1mM $MgCl_2$; pH 7.4

Drosophila buffer: 130 mM NaCl, 5 mM HEPES, 36 mM sucrose, 2 mM $CaCl_2$, 5 mM KCl, 2 mM $MgCl_2$; pH 7.4

Paraformaldehyde solution (PFA): For 500 ml PFA, 20 g PFA powder was stirred with 450 ml ddH_2O at 60°C until dissolved. If necessary, a few drops of 1 M NaOH were added to facilitate the process. 50 ml 10 x PBS were added, and pH adjusted to 7-8. The solution was aliquoted and stored at -20°C until use.

fDMEM: 10 mM MgCl2, 5 mM HEPES in DMEM

tst-binding buffer: 50 mM HEPES, 300 mM NaCl, 1 mM EDTA, pH8

tst-elution buffer: 50 mM HEPES, 300 mM NaCl, 7.5 mM dethiobiotin; pH 8

Mowiol: For 100 ml Mowiol mounting medium, 24 g Glycerol and 9.6 g Mowiol were mixed with a magnetic stirrer for 1 hour, before adding 62.4 ml distilled water and 0.6 ml 1M Tris buffer pH 8.5. The mixture was left stirring overnight, or until dissolved

4.4 Flies

Husbandry: Fruit flies *(Drosophila melanogaster)* were reared at 25°C on a 12-hour light-dark-cycle on standard corn meal medium. Adults were transferred to vials with fresh food every 2-3 weeks.

Fly lines: elav^{c155}-gal4(x) (BDSC stock Nr. 458); uas-synaptopHlourin III (Miesenböck et al. 1998)

Cross setup: Vials of elav^{c155}-gal4 flies were emptied of adult flies in the morning, and virgin females were collected periodically over the next 6-8 hours. New vials were populated with 5-10 virgin elav^{c155}-gal4(x) females and 5-10 uas-synaptopHlourin III males.

Preparation of larval fillets: For observation of the Drosophila larval neuromuscular junction, larval body wall muscle fillets were prepared as previously described (Jan and Jan 1976). Briefly, 3rd instar larvae were pinned on Silicone dishes immersed in Drosophila buffer and cut open among the dorsal midline. Internal organs and basal ganglion were removed using fine forceps and the larvae were spread open using additional pins.

4.5 Hippocampal neuronal Cultures

For generation of neuronal cultures, newborn rats (P1-P2) were decapitated and the hippocampi were removed and collected in HBSS. To aid in the extraction of neuronal cells, hippocampi were incubated in enzyme solution for 1 h (0.5 mg/ml L-cysteine, 100 mM $CaCl_2$, 50 mM EDTA, 2.5 U/ml papain, in DMEM), followed by enzyme inactivation for 15 minutes (0.2 mg/ml albumin, 0.2 mg/ml trypsin inhibitor, 10% FCS, in DMEM), and mechanical disruption. Approximately 80,000 cells/cm^2 were seeded onto 18 mm glass coverslips previously treated with nitric acid and subsequent thorough washing, sterilization, and coating with 1 mg/ml PLL. Cells were incubated in plating medium (10% horse serum, 3.3 mM glucose, 2 mM glutamine in DMEM) for 1-4 h at 37 °C before exchange of the medium to cell culture medium (B27 supplement 1:50, GlutaMAX 1:100, pen/strep 1:500, in Neurobasal-A). Cultures were maintained at 37°C and 5% CO_2.

4.6 Transfections

Transfection: Neuronal cultures were transfected with the constructs indicated via lipofectamine transfection. Coverslips were transferred to 400 µl prewarmed fDMEM per well and incubated at 37°C for 20-30 minutes. Transfection mix was prepared by mixing 23 µl optiMEM and 2 µl lipofectamine per coverslip to be transfected, as well as 1 µg DNA and optiMEM to a total volume of 25 µl per coverslip. DNA and lipofectamine mixtures were incubated separately for 5 min, before being combined and incubated for a further 20 minutes (both at room temperature). 50 µl of transfection mix was applied to each coverslip, and incubated for 20 minutes at 37°C. Subsequently, the coverslips were washed 2x with 1 ml fDMEM each, and placed back in their old medium. Cultures were allowed to express the fusion constructs for 3-10 days before being used for experiments.

4.7 Electrical stimulation

Electrical stimulation trains were applied using an A310 AccupulserTM triggered by an A385 Stimulus Isolator (both World Precision Instruments, Berlin, Germany) attached to a platinum wire electrode (custom made from from workshop at Max Planck Institute for Biophysical Chemistry, Göttingen, Germany) immersed in Tyrode (neuronal cultures), or Drosophila buffer (*Drosophila* larval fillets). A stimulation time of 10 s at 50 Hz corresponds to ~200 AP, and 30 s at 50 Hz to ~600 AP.

4.8 Surface blocking and labelling

Neuronal cultures: For surface blocking, coverslips were incubated in 100 µl divalent-free Tyrode withadded $sdAb_{GFP}$ upside down in a humidifying chamber at 37°C for 5 minutes. Samples were briefly washed with Tyrode, transferred to a 35 mm Silicone-filled petri dish filled with 37°C Tyrode, and electrically stimulated. Tyrode was removed and samples were labelled

by adding 150 µl $sdAb_{GFP}$* (diluted in divalent-free Tyrode) for 10 s, and subsequently washed by dipping in ice-cold divalent-free Tyrode before proceeding with fixation.

Drosophila larval fillets: Surface blocking was carried out by incubating larval fillets pinned on a Silicone-filled petri dish with 100 µl $sdAb_{GFP}$ diluted in Drosophila buffer for 10 minutes. Fillets were briefly washed with Drosophila buffer, 2 ml buffer were added to the petri dish, and samples were electrically stimulated. Buffer was removed and samples were labelled by adding 100 µl $sdAb_{GFP}$* in Drosophila buffer for 2 minutes, and washed briefly with Drosophila buffer before proceeding to fixation.

4.9 Immunostaining

Unless otherwise indicated, samples were fixed in a mixture of 4% PFA and 0.2 % Glutaraldeyhde on ice for 25 minutes (neuronal cultures)/30 minutes (*Drosophila* larval fillets), followed by 20 min/30 min fixation at room temperature. Samples were briefly washed three times with quenching solution (100 mM ammonium chloride, 100 mM glycine, in PBS) and incubated in quenching solution for a further 20 min/30 min. Blocking and permeabilization was carried out by washing three times for 5 min/10 min with blocking solution (1.5 % BSA, 0.1 % Triton-X 100/0.5 % Triton-X 100, in PBS). Primary and secondary antibodies were applied at the concentrations indicated in Table 1 for 1 hour each at RT in a humidifying chamber. Between antibody applications, the samples were washed three times 5 min/10 min with blocking solution. Following secondary antibody incubation, samples were washed 3 times 5 min/10 min with HS-PBS and two times 5 min/10 min in PBS, and for larval preparations, the remaining parts of head and tail of the fillets were removed, before proceeding to sample embedding/mounting.

4.10 Sample embedding/mounting

Mowiol: Neuronal culture samples were mounted by placing coverslips cell-side down on a drop (8 µl) of Mowiol on a glass microscopy slide. For larval preparations, samples were placed on a glass slide muscle-side up, excess water was removed with filter paper, a drop of Mowiol was added and a glass coverslip placed on top. Mowiol mounted samples were dried at 37°C for 40 minutes or overnight at room temperature.

TDE: Fixed/immunostained larval preparations were incubated for 10 minutes each in increasingly concentrated thio-diethanol (TDE; 30%, 50%, 70%, 90%, 3 x 100%), and mounted between two glass coverslips (one 18 mm, one 30 mm) that were sealed with picodent twinsil speed 22 (Picodent, Wipperfürth, Germany)

Melamine: Per sample, 8 mg p-Toluene were thoroughly vortexed in 96 µl H_2O. Melamine powder (224 mg per sample) was added, and the solution was incubated on a rotating platform at 250 rpm for 1 hour (or until completely dissolved). Larval preparations were dried by briefly

dabbing them with tissue paper, then dipped in Melamine solution and placed on an 18 mm coverslip muscle-side down. Samples were incubated overnight at room temperature. Subsequently, a BEEM capsule was cut at the end to generate a plastic cylinder, placed on top of the coverslip with the sample centered, and some drops of Melamine were added (approximately 3 mm high in the capsule). Samples were then incubated at 40°C for 1 day, before adding EpoFix Resin to fill the rest of the capsule, and incubated a further 3 days at 60°C. After the first 2 days at 60°C, the coverslips and BEEM capsules were removed, and the melamine was cut into a shape resembling a pyramid with the larval preparation on top, using a razor blade. All incubation steps were performed in a plastic receptable filled with Silica beads approximately 1 cm high, in order to keep air humidity low. Samples were then processed into 200 nm sections using an EM UC6 ultramicrorome (Leica, Wetzlar, Germany). Sections were collected on 12 mm glass coverslips and mounted glass slides with 4 µl Mowiol.

4.11 Imaging

Epifluorescence: Epifluorescence images were acquired with an Olympus IX71 microscope (Olympus, Hamburg, Germany) using a 60x 1.35 NA objective or a 100 x 1.45 NA TIRF objective (Olympus), as indicated, and an F-View II CCD camera (1376 x 1032 pixels; pixel size 6.45 x 6.45 µm). Excitation and emission filters for the fluorophores used are listed in Table 3.

Table 3: Filter sets used in epifluorescence imaging

channel	excitation filter	emission filter	beam splitter	catalogue number*
green	480/40 HQ	527/30 HQ	505 LP Q	F41-054
orange	545/30 HQ	610/75 HQ	570 LP Q	F41-007
red	620/60 HQ	700/75 HQ	660 LP Q	F41-008

*all from AHF, Tübingen, Germany

STED: Stimulated Emission-Depletion (STED) and confocal images were acquired using a Leica TCS STED system (Leica Microsystems GmbH, Mannheim, Germany) with a 100x 1.4 NA objective (100x HCX PL APO CS oil; Leica Microsystems). For STED images a 635 nm pulsed diode laser (PicoQuant, Berlin, Germany) was used to excite the fluorophores, and a Spectra-Physics MaiTai multiphoton laser at 750 nm (Newport Spectra-Physics, Santa Clara, CA, USA) was used for depletion. Fluorescence was detected with an Avalanche photodiode (APD, Leica Microsystems). For confocal images, the 488 nm line of a helium-neon laser was used for excitation in the green channel (GFP, Atto-488, Alexa 488), and the 546 line of an argon laser for excitation in the orange channel (Cy3). Fluorescence was detected by a

Photomultiplier gated by a resonance scanner for the appropriate emission windows of the fluorophores.

4.12 Image Analysis

Image analysis was performed using custom-written MATLAB routines (The Mathworks Inc., Natick, MA, USA).

For quantification of Atto647 and GFP fluorescence intensities from epifluorescence images in overall synaptic boutons, boutons were selected manually, mean fluorescence intensities in the selected areas were corrected for a likewise selected background, and the ratios of Atto647 to GFP fluorescence were calculated bouton-wise.

STED images from $sdAb_{GFP}$* labelled samples were median and average filtered to remove noise, and the locations of fluorescent spots were identified by an empirically determined intensity threshold over background. In the unprocessed STED images, Lorentzian distribution functions centered on these locations were then fit on line scans in x and y directions, and the FWHM and peak intensity returned were calculated as the means of these values from both Lorentzian fits.

References

Balaji, J. and T. A. Ryan. 2007. “Single-Vesicle Imaging Reveals That Synaptic Vesicle Exocytosis and Endocytosis Are Coupled by a Single Stochastic Mode.” *Proceedings of the National Academy of Sciences* 104(51):20576–81. Retrieved (http://www.pnas.org/cgi/doi/10.1073/pnas.0707574105).

Denker, A., K. Krohnert, J. Buckers, E. Neher, and S. O. Rizzoli. 2011. “The Reserve Pool of Synaptic Vesicles Acts as a Buffer for Proteins Involved in Synaptic Vesicle Recycling.” *Proceedings of the National Academy of Sciences* 108(41):17183–88. Retrieved (http://www.pnas.org/cgi/doi/10.1073/pnas.1112690108).

Dreosti, Elena and Leon Lagnado. 2011. “Optical Reporters of Synaptic Activity in Neural Circuits.” *Experimental Physiology* 96(1):4–12. Retrieved June 17, 2017 (http://doi.wiley.com/10.1113/expphysiol.2009.051953).

Fernández-Alfonso, Tomás, Ricky Kwan, and Timothy A. Ryan. 2006. “Synaptic Vesicles Interchange Their Membrane Proteins with a Large Surface Reservoir during Recycling.” *Neuron* 51(2):179–86.

Fornasiero, Eugenio F. and Felipe Opazo. 2015. “Super-Resolution Imaging for Cell Biologists: Concepts, Applications, Current Challenges and Developments.” *BioEssays : News and Reviews in Molecular, Cellular and Developmental Biology* 37(4):436–51. Retrieved June 19, 2017 (http://doi.wiley.com/10.1002/bies.201400170).

Granseth, Björn, Benjamin Odermatt, Stephen J. Royle, and Leon Lagnado. 2006. “Clathrin-Mediated Endocytosis Is the Dominant Mechanism of Vesicle Retrieval at Hippocampal Synapses.” *Neuron* 51(6):773–86.

Haucke, Volker, Erwin Neher, and Stephan J. Sigrist. 2011. “Protein Scaffolds in the Coupling of Synaptic Exocytosis and Endocytosis.” *Nature Reviews. Neuroscience* 12(3):127–38. Retrieved February 19, 2014 (http://www.ncbi.nlm.nih.gov/pubmed/21304549).

Hoopmann, Peer et al. 2010. “Endosomal Sorting of Readily Releasable Synaptic Vesicles.” *Proceedings of the National Academy of Sciences of the United States of America* 107:19055–60.

Jan, Y. N. and L. Y. Jan. 1976. “Properties of the Larval Neuromuscular Junction in Drosophila Melanogaster.” 262:189–214.

Maidorn, M., S. O. Rizzoli, and F. Opazo. 2016. “Tools and Limitations to Study the Molecular Composition of Synapses by Fluorescence Microscopy.” *Biochemical Journal* 473(20):3385–99. Retrieved (http://biochemj.org/cgi/doi/10.1042/BCJ20160366).

Miesenböck, G., D. A. De Angelis, and J. E. Rothman. 1998. “Visualizing Secretion and Synaptic Transmission with pH-Sensitive Green Fluorescent Proteins.” *Nature* 394(6689):192–95. Retrieved June 17, 2017 (http://www.nature.com/doifinder/10.1038/28190).

Opazo, Felipe et al. 2010. “Limited Intermixing of Synaptic Vesicle Components upon Vesicle Recycling.” *Traffic* 11(6):800–812.

Opazo, Felipe and Silvio O. Rizzoli. 2010. “The Fate of Synaptic Vesicle Components upon Fusion.” *Communicative & Integrative Biology* 3(April 2015):427–29.

Ries, Jonas, Charlotte Kaplan, Evgenia Platonova, Hadi Eghlidi, and Helge Ewers. 2012. “A Simple, Versatile Method for GFP-Based Super-Resolution Microscopy via Nanobodies.” *Nature Methods* 9(6):582–84. Retrieved June 5, 2014 (http://www.ncbi.nlm.nih.gov/pubmed/22543348).

Rizzoli, Silvio O. 2014. “Synaptic Vesicle Recycling.” 33(8):2014.

Rothbauer, Ulrich et al. 2006. “Targeting and Tracing Antigens in Live Cells with Fluorescent Nanobodies.” *Nature Methods* 3(11):887–89. Retrieved June 17, 2017 (http://www.nature.com/doifinder/10.1038/nmeth953).

Ryan, Timothy A., Stephen J. Smith, Harald Reutert, and Charles F. Stevens. 1996. “The Timing of Synaptic Vesicle Endocytosis.” *Neurobiology* 93(May):5567–71.

Sankaranarayanan, S. and T. A. Ryan. 2001. “Calcium Accelerates Endocytosis of vSNAREs at Hippocampal Synapses.” *Nature Neuroscience* 4(2):129–36. Retrieved June 17, 2017 (http://www.nature.com/doifinder/10.1038/83949).

Sankaranarayanan, Sethuraman and Timothy A. Ryan. 2000. “Real-Time Measurements of Vesicle- SNARE Recycling in Synapses of the Central Nervous System.” *Nature Cell Biology* 2(April):197–204.

Sinha, Raunak. 2011. “Optical Analysis of Synaptic Vesicle Protein Molecules during Exo - and Endocytosis Using pH - Switchable Fluorescent Probes PhD Thesis.” University of Göttingen.

Takamori, Shigeo et al. 2006. *Molecular Anatomy of a Trafficking Organelle*.

Vreja, Ingrid C. et al. 2015. “Super-Resolution Microscopy of Clickable Amino Acids Reveals the E Ff Ects of Fluorescent Protein Tagging on Protein Assemblies.” (11):11034–41.

Westphal, V. et al. 2008. “Video-Rate Far-Field Optical Nanoscopy Dissects Synaptic Vesicle Movement.” *Science* 320(5873):246–49. Retrieved (http://www.sciencemag.org/cgi/doi/10.1126/science.1154228).

Wienisch, Martin and Jurgen Klingauf. 2006. “Vesicular Proteins Exocytosed and Subsequently Retrieved by Compensatory Endocytosis Are Nonidentical.” *Nature Neuroscience* 9(8):1019–27. Retrieved (http://www.ncbi.nlm.nih.gov/pubmed/16845386).

Wilhelm, B. G. et al. 2014. “Composition of Isolated Synaptic Boutons Reveals the Amounts of Vesicle Trafficking Proteins.” *Science* 344(6187):1023–28. Retrieved May 29, 2014 (http://www.sciencemag.org/cgi/doi/10.1126/science.1252884).

Willig, Katrin I., Silvio O. Rizzoli, Volker Westphal, Reinhard Jahn, and Stefan W. Hell. 2006. “STED Microscopy Reveals That Synaptotagmin Remains Clustered after Synaptic Vesicle Exocytosis.” *Nature* 440(7086):935–39. Retrieved (http://www.nature.com/doifinder/10.1038/nature04592).

Wu, L. G. and W. J. Betz. 1996. “Nerve Activity but Not Intracellular Calcium Determines the Time Course of Endocytosis at the Frog Neuromuscular Junction.” *Neuron* 17(4):769–79. Retrieved June 19, 2017 (http://www.ncbi.nlm.nih.gov/pubmed/8893033).

List of Figures

List of Tables

List of Abbreviations

AP	action potential
brp	bruchpilot
BSA	bovine serum albumine
DIV	day in vitro
DMEM	Dulbecco's modified Eagle's Medium
dNMJ	Drosophila melanogaster neuromuscular junction
FCS	fetal calf serum
PBS	phosphate-buffered saline
pdf	probability distribution function
PFA	paraformaldehyde
ROI	region of interest
sdAb	single-domain antibody
spH	synaptophysin-pHluorin
STED	stimulated emission-depletion
sypHy	synaptobrevin-pHluorin
TDE	thio-diethanol